Product Datasheet

HIF-2 alpha/EPAS1 Antibody - BSA Free
NB100-122

Unit Size: 0.1 ml

Store at -20 °C.

www.novusbio.com technical@novusbio.com

Reviews: 37 Publications: 781

Protocols, Publications, Related Products, Reviews, Research Tools and Images at:
www.novusbio.com/NB100-122

Updated 6/25/2024 v.20.1

Earn rewards for product reviews and publications.
Submit a publication at www.novusbio.com/publications
Submit a review at www.novusbio.com/reviews/destination/NB100-122

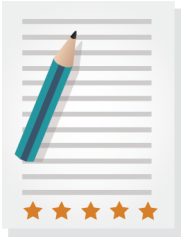

NB100-122

HIF-2 alpha/EPAS1 Antibody - BSA Free

Product Information	
Unit Size	0.1 ml
Concentration	1.0 mg/ml
Storage	Store at -20 °C.
Clonality	Polyclonal
Preservative	0.05% Sodium Azide
Isotype	IgG
Purity	Immunogen affinity purified
Buffer	PBS
Target Molecular Weight	96.5 kDa

Product Description	
Host	Rabbit
Gene ID	2034
Gene Symbol	EPAS1
Species	Human, Mouse, Rat, Fish, Hamster, Primate, Rabbit, Reptile, Sheep
Reactivity Notes	Use in Mouse reported in scientific literature (PMID:33758176).
Specificity/Sensitivity	This HIF-2 alpha/EPAS1 Antibody is specific for HIF-2 alpha/EPAS, and does not cross-react with HIF-1 alpha.
Immunogen	This HIF-2 alpha/EPAS1 Antibody was developed against a peptide derived from the C-terminus of mouse/human HIF-2 alpha protein.

Product Application Details	
Applications	Western Blot, Simple Western, ELISA, Flow Cytometry, Gel Super Shift Assays, Immunoblotting, Immunocytochemistry/ Immunofluorescence, Immunohistochemistry, Immunohistochemistry-Frozen, Immunohistochemistry-Paraffin, In vitro assay, Immunoprecipitation, SDS-Page, Chromatin Immunoprecipitation (ChIP), Dual RNAscope ISH-IHC, Knockdown Validated, Knockout Validated
Recommended Dilutions	Western Blot 1 - 2 ug/mL, Simple Western 1:50, Flow Cytometry, ELISA 1:100 - 1:2000, Immunohistochemistry 1:100, Immunocytochemistry/ Immunofluorescence 1:100, Immunoprecipitation 5 ug / 1 mg lysate, Immunohistochemistry-Paraffin 1:100, Immunohistochemistry-Frozen, Immunoblotting reported in scientific literature (PMID 28115701), In vitro assay reported in scientific literature (PMID 24998849), Gel Super Shift Assays reported in scientific literature (PMID 15184875), SDS-Page, Chromatin Immunoprecipitation (ChIP) 1:10-1:500, Knockout Validated reported in scientific literature (PMID 26861754), Knockdown Validated reported in scientific literature (PMID 31061092), Dual RNAscope ISH-IHC
Application Notes	In WB, this antibody recognizes a band at 118 kDa representing HIF-2 alpha. Simple Western reported by an internal validation. Separated by Size- Wes/Sally Sue/Peggy Sue, antibody dilution of 1:50. Apparent MW in kDa on Simple Western was 110kDa; matrix was 12-230 kDa.

Images

WNT11 is induced by hypoxia or hypoxic mimetics in different cell types. Immunoblot analyses of HeLa cells under normal air or hypoxia for 24 hrs. Image collected and cropped by CiteAb from the following publication (https://www.nature.com/articles/srep21520) licensed under a CC-BY license.	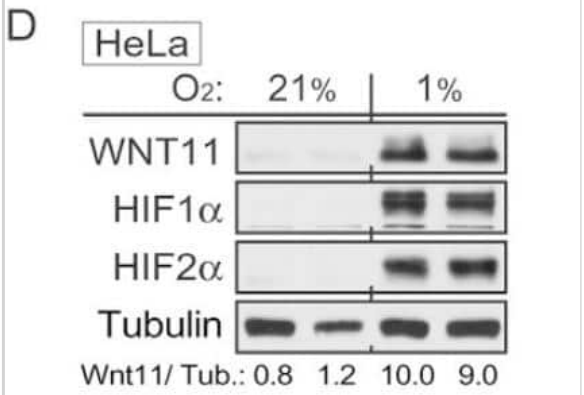
HIF-1alpha is the predominant transcriptional regulator of WNT11 expression during hypoxia. EMSCs isolated from the indicated mouse genotypes were infected with lentivirus expressing GFP or Cre recombinase. Non-infected cells and GFP infected cells served as controls. Immunoblot analyses of EMSCs derived from the indicated genotypes treated with 0.1 mM DMOG for 24 hrs. Attenuated WNT11 expression in Hif-1alpha KO EMSCs (lenti-Cre infected Hif-1af/f). Image collected and cropped by CiteAb from the following publication (https://www.nature.com/articles/srep21520) licensed under a CC-BY license.	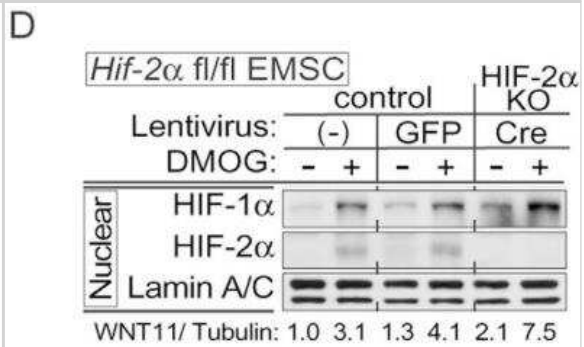
Formalin-fixed paraffin-embedded tissue sections of human placenta were probed for HIF-2 alpha/EPAS1 mRNA (ACD RNAScope Probe, catalog #410598; Fast Red chromogen, ACD catalog # 322750). Adjacent tissue section was processed for immunohistochemistry using Rabbit Polyclonal (Novus Biologicals catalog # NB100-122) at 1:100 dilution with one-hour incubation at room temperature followed by incubation with anti-rabbit IgG VisUCyte HRP Polymer Antibody (Catalog # VC003) and DAB chromogen (yellow-brown). Tissue was counterstained with hematoxylin (blue). Specific staining was localized to trophoblastic cells.	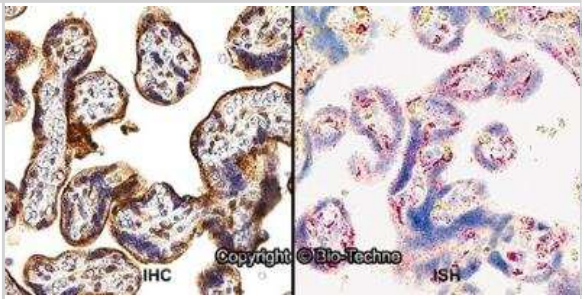
Expression of hypoxia-inducible alpha subunits in normal and diseased lung tissue. HIF-2alpha expression are more evident in fibroblasts from idiopathic pulmonary fibrosis (d) than from lung tissue affected by other inflammatory conditions (i.e. chronic bronchitis, panel e) or normal lung tissue (f); as demonstrated by a higher proportion of positive fibroblasts (open arrows) than negative ones (solid black arrows). Image collected and cropped by CiteAb from the following publication (https://respiratory-research.biomedcentral.com/articles/10.1186/s12931-019-1100-4) licensed under a CC-BY license.	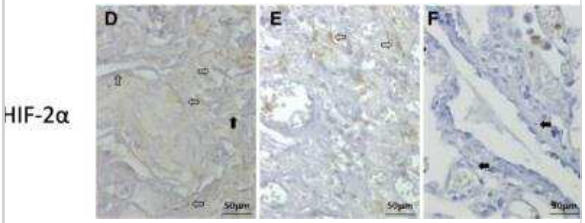

Image shows a specific band for HIF-2 alpha in 0.5 mg/mL of hypoxic HeLa lysate. This experiment was performed under reducing conditions using the 12-230 kDa separation system.	
Immunoblot validation of HIF2A and PHD2 KO clones using HIF2A (#NB100-122; dilution: 1/300), PHD2 (#NB100-137; dilution: 1/500). To blot HIFs factor cells were first pre-treated for 5 h with CoCl2 300 uM before protein extraction, a condition that promotes HIF factor accumulation. Image collected and cropped by CiteAb from the following publication (https://www.nature.com/articles/s41467-018-06988-3) licensed under a CC-BY license.	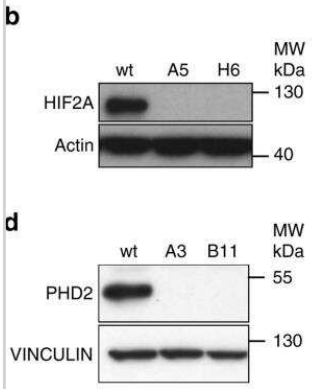
HIF-2 alpha in human retinal and choroidal primary endothelia lysates using .. Image from verified customer review.	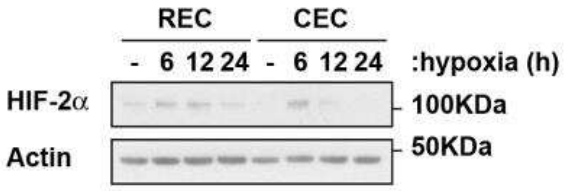
HIF-2 alpha in MDA-MB-231 cell lysate (overexpression and endogenous samples) using . did not react to HIF-1 alpha overexpression. Image from verified customer review.	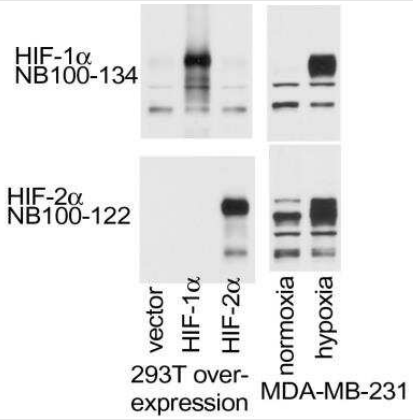

Induced WNT11 expression with tumor hypoxia and WNT11 regulates tumor growth. Bevacizumab increased expression of HIF-1alpha and HIF-2alpha and WNT11. First 10 lanes are control tumors, and the last 10 lanes are tumors from bevacizumab-treated animals. Lysates from whole tissue and nuclei are indicated. Alpha -Tubulin, actin and lamin A/C are loading controls. Image collected and cropped by CiteAb from the following publication (https://www.nature.com/articles/srep21520) licensed under a CC-BY license.	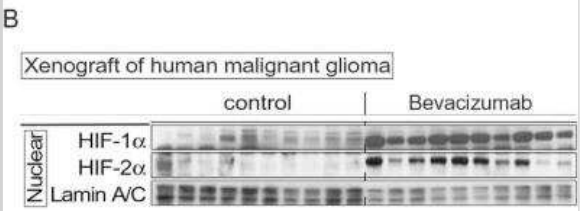
MDA-MB-231 cells were exposed to 20% or 1% O2 for 16 hours, and chromatin immunoprecipitation (ChIP) was performed with the indicated antibody (Ab). Primers flanking the HIF binding site were used for qPCR. ChIP image submitted by a verified customer review.	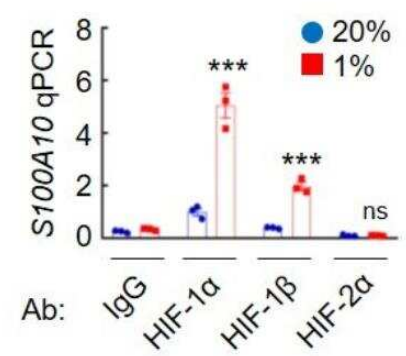
Lane 1: Cobalt chloride treated COS7 nuclear extracts. Lane 2: Untreated COS7 nuclear extracts.	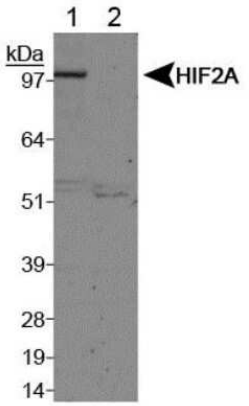
786-O cells without or with VHL overexpression. Image from verified customer review.	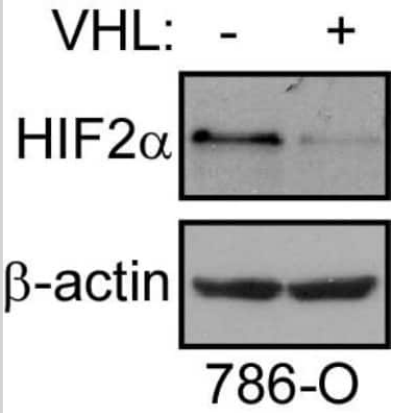

Analysis using the HRP conjugate of NB100-122. Detection of normoxic and hypoxic nuclear rat cell lysates.	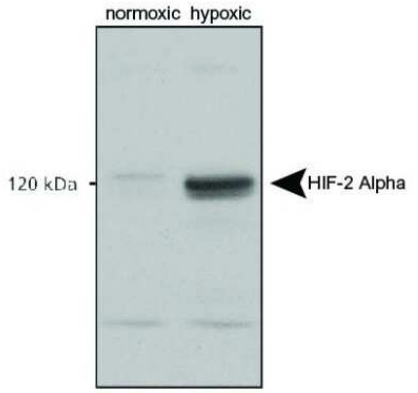
HIF-2 alpha immunoreactivity in human cardiac myocytes stained with NB100-122.	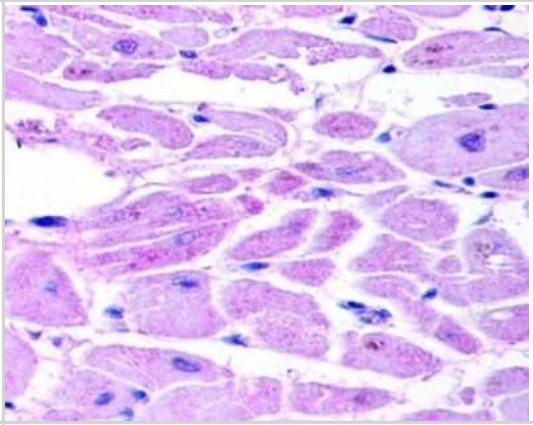
Expression and correlation of 3 antibodies: HIF-1 alpha, HIF-2 alpha and HAF in ccRCC. (A, C & E) Positive nuclear staining to the 3 antibodies: HIF-1 alpha, HIF-2 alpha and HAF, in primary ccRCCs at high magnification (100X). (B, D & F) Heterogenous nuclear staining of 3 antibodies in a tumor at low magnification (20X). (G, H and I). Correlation of 3 antibodies with the Fuhrman grade. Citation: Ambrosetti D, Dufies M, Dadone B, Durand M, Borchiellini D, Amiel J, et al. (2018) The two glycolytic markers GLUT1 and MCT1 correlate with tumor grade and survival in clear-cell renal cell carcinoma. PLoS ONE 13(2): e0193477. https://doi.org/10.1371/journal.pone.0193477	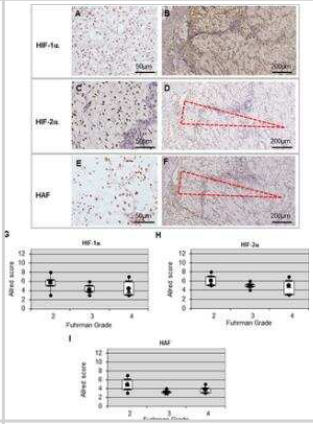
Reduction of HIF-2alpha levels leads to protection in UV-triggered apoptosis, but not for apoptosis caused by glucose and serum starvation in 786-O cells. Parental 786-O or those either stably expressing wild-type VHLp19 or stably infected with a control vector (pSuperRetro) or a pool of two HIF-2alpha shRNAs vectors [21] were grown to confluence and lysed. Cell alpha-tubulin.	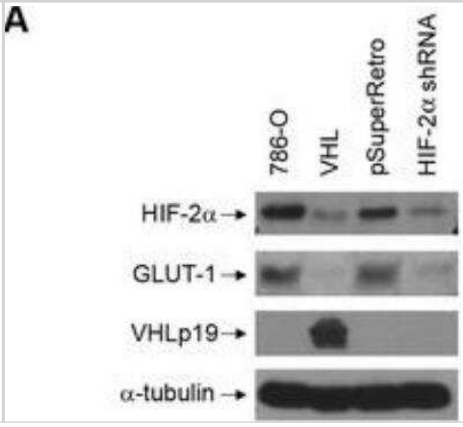

Sp1 and HIFs contribute to the synergistic activation of multiple genes in OVSAYO cells under SSH.b) Activation of multiple genes under hypoxia is dependent on HIFs. Western blotting is also shown for HIFs. Data shown are the mean (n = 3) ± SD.	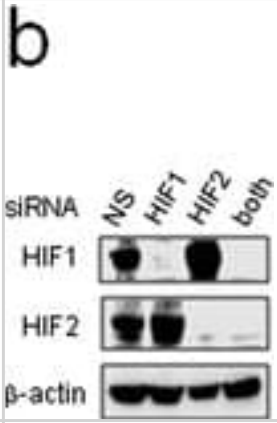
Manipulation of DNA methylation at HRE sequences alters HIF binding. (A) The Hypoxia Response Element (HRE) contains a CpG site that can be methylated which prevents HIF1 and HIF2 binding in vitro. EMSA of in vitro-translated HIF1 and HIF2 binding to 32P-labelled unmethylated and methylated HRE probes. Competition with 250X molar excess of unlabelled/unmethylated HRE probe (lanes 3, 7,12, 16) or unlabelled control HRE-free probe (lanes 4, 8, 13, 17). HIF1 and HIF2 complexes bound to unmethylated HRE or methylated HRE supershifted with anti-HIF1alpha (lanes 9 and 18) and anti-HIF2alpha (lanes 5 and 14). Image collected and cropped by CiteAb from the following publication (https://www.nature.com/articles/s41598-018-21524-5), licensed under a CC-BY licence.	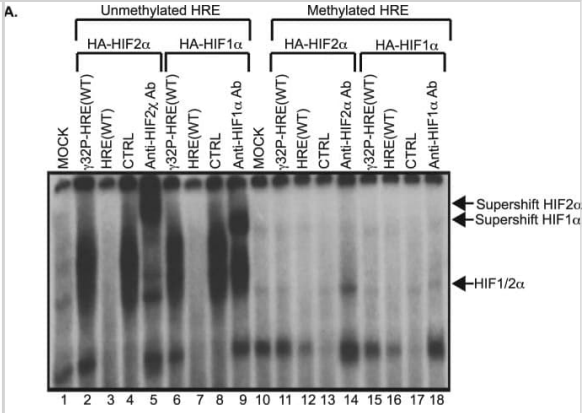
Hypoxia and HIF-1 accumulation after DSS-treatment.Real time PCR of HIF-1alpha exon 2 (A) in RNA samples of hypoxic treated BMDM of wild type (HIF-1alpha+f/+f) and knockout (Lyz2-Cre/HIF-1alpha+f/+f) mice with 14 samples/group. Each bar represents the mean value +/- SEM. ***P < 0.001. Immunohistochemical staining of hypoxia with Hypoxyprobe-1 (HP-1) antibody (B) or staining of HIF-1alpha (C) and HIF-2alpha (D) in paraffin-embedded colon tissue of wild type (HIF-1alpha+f/+f) and knockout (Lyz2-Cre/HIF-1alpha+f/+f) mice after treatment with drinking water (C = control) or with 2.5% DSS for six days (6d). Note, that the HIF-1alpha antibody recognizes both wild type and knockout HIF-1alpha (lacking exon 2) and therefore detects (non-functional) HIF-1alpha protein in knockout mouse tissue. Representative images of stained colon slices of experiments with five or six mice/group. Original bars 100 um. Image collected and cropped by CiteAb from the following publication (https://dx.plos.org/10.1371/journal.pone.0190074), licensed under a CC-BY licence.	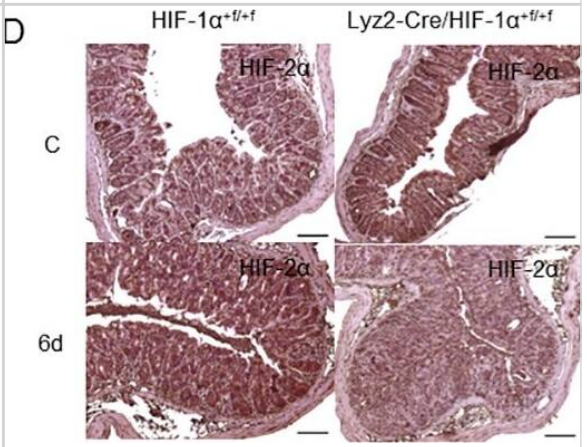
Representative immunoblots with specific detection of HIF-1alpha, HIF-2alpha in nuclear protein extracts and VEGFR-1, VEGFR-2, and VEGF in total protein extracts obtained at four weeks of age.In response to hypoxia sham operated animals showed apparent activation of HIF-1alpha and HIF-2alpha based upon increased nuclear protein concentrations, along with increased expression of VEGFR-1 and VEGFR-2. Pressure load appeared to increase HIF-1alpha activation and perhaps modestly increase VEGRF-1 expression, without changing HIF-2alpha activation. LV hypertrophy prevented hypoxia-induced increases in HIF-2alpha activation, decreased VEGFR-2 expression, and increased VEGFR-1 expression. VEGF levels were not affected by hypoxia or aortic banding. Image collected and cropped by CiteAb from the following publication (https://pubmed.ncbi.nlm.nih.gov/19112498), licensed under a CC-BY licence.	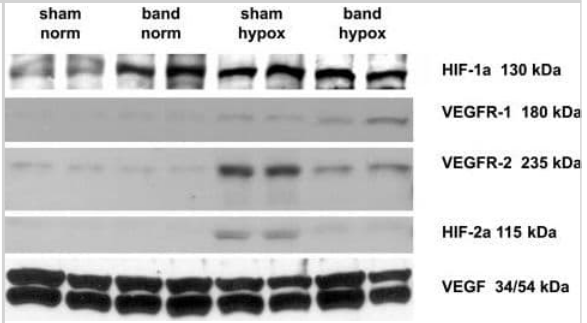

HIF-1alpha and HIF-2alpha are reduced by HFD and SIRT3 loss in the heart. WT and SIRT3 KO mice were fed ND or HFD for 16 weeks. Hearts were extracted and Western blot analysis was performed on ventricular lysates. (B) Representative blots of HIF-2alpha and GAPDH. Values are mean +/- SEM (n = 6 ND and 5-7 HFD). PI = ns, PD <= 0.05, PS <= 0.01; *P <= 0.05; **P <= 0.01. Image collected and cropped by CiteAb from the following publication (https://pubmed.ncbi.nlm.nih.gov/25782072), licensed under a CC-BY licence.

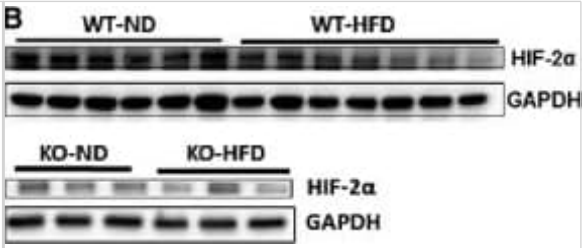

Chronic hypoxia promotes ceramide hydrolytic metabolism by activating the HIF-2alpha/Acer2 signaling pathway, thereby downregulating PP2A activity. F-I) The levels of HIF-1alpha, HIF-2alpha, and Acer2 in the nuclei of the hippocampi of mice of different hypoxic time groups (Con, H1d, H3d, H7d, H14d) were detected by western blots with beta-actin as the internal reference; Statistical analysis was performed. Image collected and cropped by CiteAb from the following publication (https://pubmed.ncbi.nlm.nih.gov/36450714), licensed under a CC-BY licence.

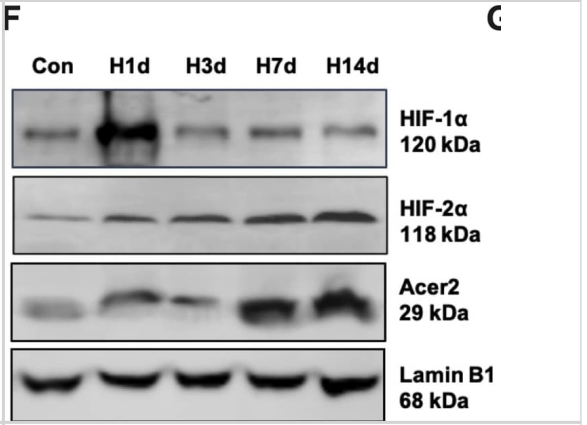

HIF-1alpha activates transcription of Sox17. a) Western blot analysis in control HLMVECs and HLMVECs for which CRISPR/Cas9 was used to delete HIFs. ECs were treated with the HIF prolyl hydroxylase inhibitor DMOG to induce HIF expression. DMOG (1 mM) increased HIF-1alpha and HIF-2alpha protein expression in control ECs but not in ECs lacking HIF-1alpha or HIF-2alpha. Induction of HIF expression was coupled to Sox17 upregulation. n = 3. Image collected and cropped by CiteAb from the following publication (https://pubmed.ncbi.nlm.nih.gov/31073164), licensed under a CC-BY licence.

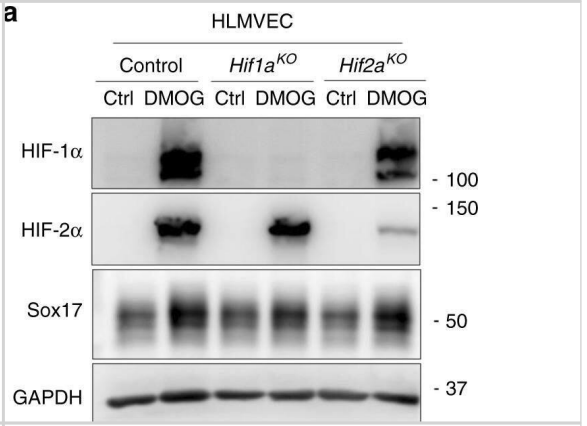

Oxygen Consumption Rate (OCR), Extracellular Acidification Rate (ECAR) of C2C12, and wild-type and FTO knockout MEFs treated with 1 uM IOX3 or an equivalent amount of vehicle control for 16 hours. E) Expression of FTO, phosphorylated-AMPKalpha and HIF-1alpha with representative ACTIN in cells treated with vehicle, 1uM IOX3, control scrambled siRNA or Fto siRNA for 24 hours. N = 3 biological replicates per condition. Image collected and cropped by CiteAb from the following publication (https://dx.plos.org/10.1371/journal.pone.0121829), licensed under a CC-BY licence.

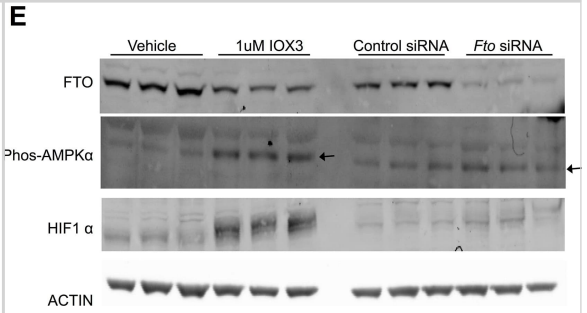

Validation of endogenous HIF2A reporter systems. (c) Western blot analysis of H2AmC2 and H2AmC3 dCas9 cells transduced with HIF2A-targeting sgRNAs or a non-targeting control. B-actin acts as a loading control. Full-length blots are presented in Supplementary Fig. 5. Image collected and cropped by CiteAb from the following publication (https://pubmed.ncbi.nlm.nih.gov/30104738), licensed under a CC-BY licence.	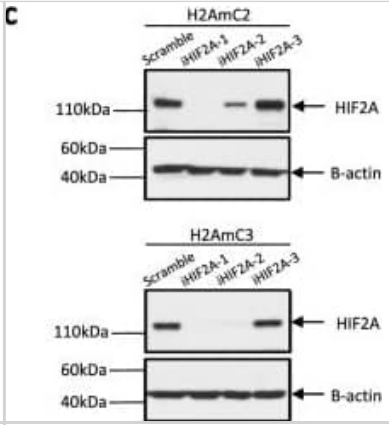
HIF2A modulates KLF6 expression in ccRCC. C) KLF6, HIF2A and VHL immunoblot of cells transduced with HA-VHL or empty vector. Representative of three experiments for 786-M1A and two for OS-LM1 cells. Image collected and cropped by CiteAb from the following publication (https://pubmed.ncbi.nlm.nih.gov/30858363), licensed under a CC-BY licence.	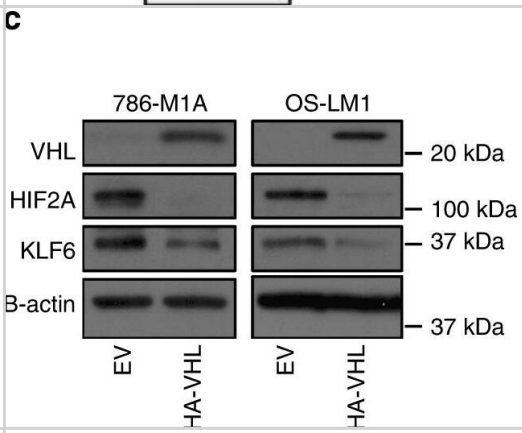
CPT1A repression controls lipid deposition in ccRCC cells. A) Western blot of RCC4 cell lysates expressing shRNA to HIF1alpha and HIF2alpha decorated with antibodies to HIF1alpha, HIF2alpha, CPT1A, and beta-actin. Image collected and cropped by CiteAb from the following publication (https://www.nature.com/articles/s41467-017-01965-8), licensed under a CC-BY licence.	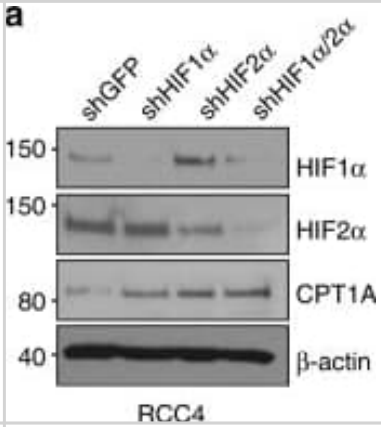
Effect of OTC or LA on levels of hypoxia-inducible factor (HIF)-1alpha, HIF-1beta, and HIF-2alpha in nuclear protein extracts from lung tissues. Sampling was performed at 48 h after the last challenge in saline-inhaled mice administered drug vehicle (SAL + VEH), OVA-inhaled mice administered drug vehicle (OVA + VEH), OVA-inhaled mice administered OTC (OVA + OTC), and OVA-inhaled mice administered LA (OVA + LA). (c) Representative Western blotting of HIF-2alpha. Image collected and cropped by CiteAb from the following publication (https://www.mdpi.com/1422-0067/13/7/7915), licensed under a CC-BY licence.	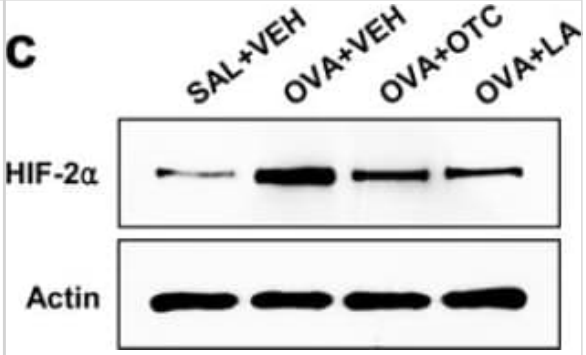

VEGF-A is highly expressed in the DSCs of pregnant uterus, but is not spatially matched with hypoxia and HIF-1alpha and HIF-2alpha expressions. .E, F Expressions of HIF-1alpha and HIF-2alpha in the uteri at 6.5 dpc. Each numbered region (square-dotted line) is magnified and arrayed in right side. Scale bars, 500 um. Image collected and cropped by CiteAb from the following publication (https://pubmed.ncbi.nlm.nih.gov/23853117), licensed under a CC-BY licence.	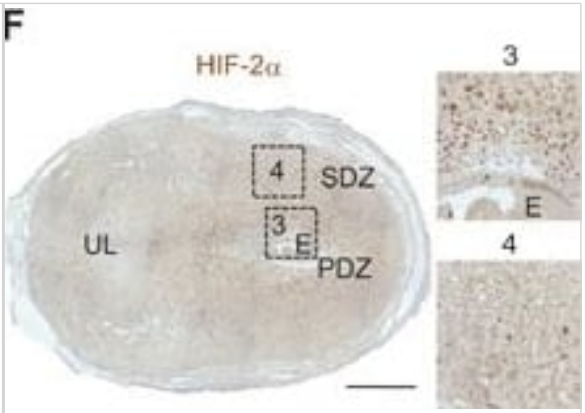
Inhibition and silencing of HIF-2alpha reduces hypoxia-mediated NFATc2 nuclear translocation. (D) Western blot showing HIF-1alpha and HIF-2alpha silencing efficiency. Image collected and cropped by CiteAb from the following publication (https://www.nature.com/articles/s41598-018-21073-x), licensed under a CC-BY licence.	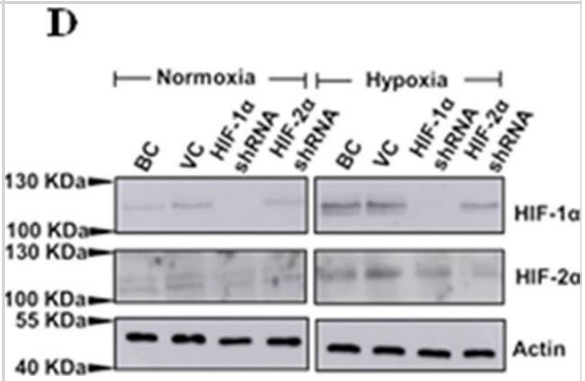
Copper deficiency anemia results in increases in duodenal hypoxia and Hif-2alpha but partial alleviation of anemia, by copper injection, reduces duodenal hypoxia and down regulates Hif-2alpha.(A) Immunoblot of Hif-2alpha (nuclear fraction). Hsc70 was used as a loading control. 1-way ANOVA with Newman-Keuls posthoc testing. CTR (n = 6), CuD (n = 6), CuD+CuSO4) (n = 4). Image collected and cropped by CiteAb from the following publication (https://pubmed.ncbi.nlm.nih.gov/23555700), licensed under a CC-BY licence.	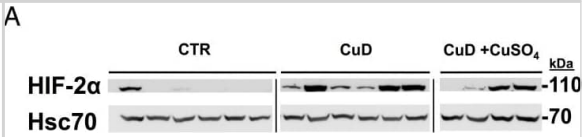

HIF2alpha stabilization results in exocrine cell atrophy and expansion of duct-like tubular structures. (A) Body weight (left panel), pancreas weight (middle panel) and body/pancreas weight ratio (right panel) in Pdx1-Cre;HIF2dPA and control mice at 2 and 8 weeks of age. Data are presented as mean +/- SD. (B) HIF2alpha accumulation in Pdx1-Cre;HIF2dPA analyzed by Western blot with anti-HA antibody. Two independent two-week-old control and mutant mice are shown. beta-actin protein was used for loading control. Full-length blots are presented in Supplementary Fig. 2. (D) Immunofluorescence analysis of HIF2alpha in two-week-old control pancreata. Endogenous HIF2alpha expression is observed in islets (marked by an white asterisk) but not in exocrine tissue. (D) Robust HIF2alpha accumulation in the pancreas of two-week-old Pdx1-Cre;HIF2dPA mice. Hematoxylin/Eosin-stained pancreatic sections from P0 (E,F), two- (I,J) and eight-week-old (M,N) Pdx1-Cre;HIF2dPA and control mice. Inset in N shows an area with adipose tissue in Pdx1-Cre;HIF2dPA pancreata. Immunofluorescence of amylase and KRT19 shows no differences between Pdx1-Cre;HIF2dPA and control mice at P0 (G,H). Duct-like tubular structures and loss of amylase immunoreactivity in two- (K,L) and eight-week-old (O,P) Pdx1-Cre;HIF2dPA mice compared to control mice. Note areas with normal acini in 8-week-old Pdx1-Cre;HIF2dPA mice (white asterisk in O). Insets in (H,L and P) show higher magnification pictures. DAPI staining is shown in blue in (C,D,G,H,K,L,O and P). Scale bars = 50 um for (C,D); 100 um for (E-P). ***P < 0.001. Image collected and cropped by CiteAb from the following publication (https://pubmed.ncbi.nlm.nih.gov/30209343), licensed under a CC-BY licence.

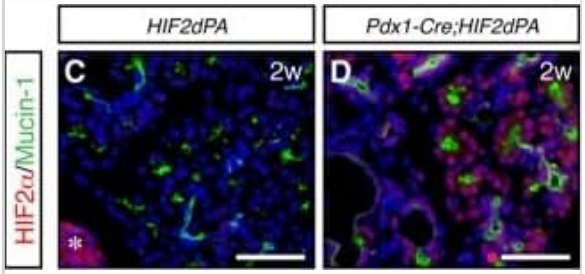

Western Blot: Rabbit Polyclonal HIF-2 alpha/EPAS1 Antibody [NB100-122] - Analysis of HIF-2 alpha/EPAS1 antibody on mouse liver nuclear extracts. Image from a verified customer review.

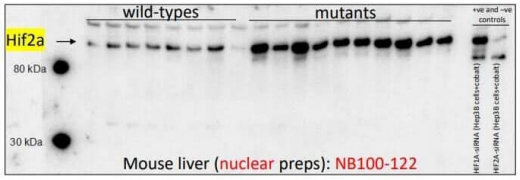

HMGB1 expression became up-regulated in thyroid cancer and was associated with clinicopathologic features (a) Western blot of HMGB1 and actin in various cell lines hinted at an over-expression of HMGB1 in thyroid cancer; (b) Immunohistochemical staining of HMGB1 was performed for different tissues. TC, thyroid cancer; TA, thyroid adenoma; SG, simple goiter; N, normal thyroid; PTC, papillary thyroid carcinoma; FTC, follicular thyroid carcinoma; (c) Relative expression levels of HMGB1 in different tissues. Total mRNA was extracted from normal or patient tissues and HMGB1 level determined by relative optical intensity (in arbitrary units, AU) of bands on RT-PCR. Each dot represented relative level of HMGB1 in each individual sample. *P < 0.01 vs. normal thyroid; **P > 0.01 vs. normal thyroid; #P > 0.01 vs. normal thyroid; (d) Relative expression levels of HMGB1 in thyroid cancer. Total mRNA was extracted from thyroid cancer patients' tissues and HMGB1 level determined by relative optical intensity (in arbitrary units, AU) of bands on RT-PCR. Each dot represented relative level of HMGB1 in an individual sample. *P > 0.01 vs. FTC; (e) HMGB1 expression level for differentiating thyroid cancer tissues from non-thyroid cancer tissues in our validated cohort; AUC: 96.7%, sensitivity: 88.9% and specificity: 96.2% in the validated cohort Image collected and cropped by CiteAb from the following open publication (https://pubmed.ncbi.nlm.nih.gov/31331356), licensed under a CC-BY license. Not internally tested by Novus Biologicals.

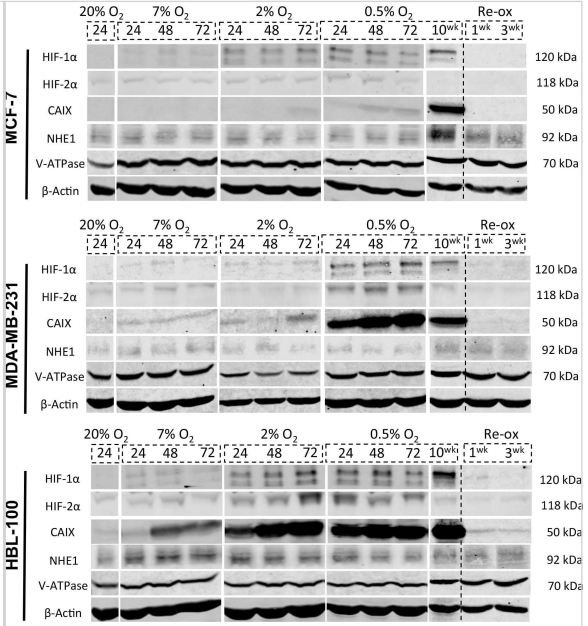

Loss of MUS81 activates DNA damage responseA. MUS81 depleted U2OS cells accumulate NBS1 foci defining sites of DNA damage. B. Partial co-localization of NBS1 foci and RPA foci in MUS81-depleted cells. C. Co-localization of RPA foci to ssDNA regions. Cells were labelled with BrdU for 3 days concomitant with MUS81 depletion. BrdU was detected at ssDNA regions by immunofluorescence. D. NBS1 foci arise in cells that are both positive and negative for Cyclin A expression. Scale bars, 5 μm. E. NBS1 foci form largely at non-telomeric loci. F. Partial co-localization of NBS1 foci with PML nuclear bodies. Image collected and cropped by CiteAb from the following open publication (https://pubmed.ncbi.nlm.nih.gov/26415217), licensed under a CC-BY license. Not internally tested by Novus Biologicals.

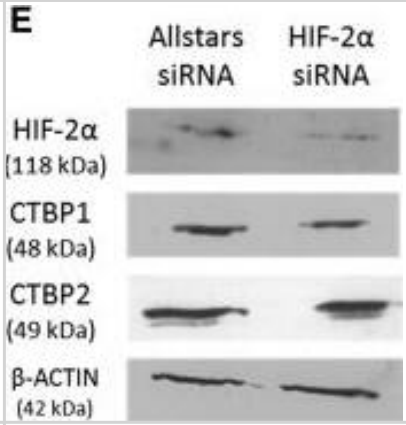

Immunohistochemical detection of HIF-1α protein in human tissues. The nature of the tissue is indicated on top of each figure. Original magnifications are as follows: A, ×400; B, ×400; C, ×100; D, ×100; E, ×100; F, ×100; G, ×40; H, ×40. Image collected and cropped by CiteAb from the following open publication (https://bmcgenet.biomedcentral.com/articles/10.1186/1471-2156-5-27), licensed under a CC-BY license. Not internally tested by Novus Biologicals.

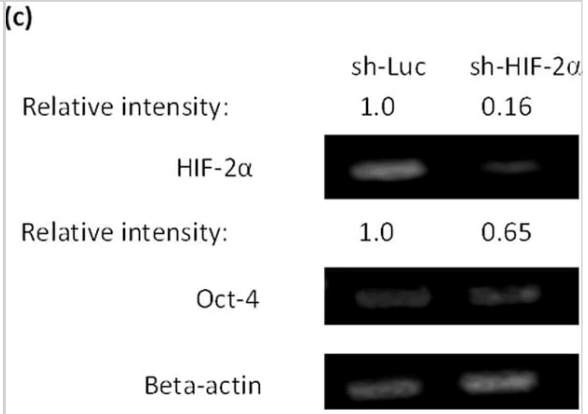

ROS overproduction mediated apoptosis induced by combined treatment of DDP and HIF-1α in PC-3 xenografts and cell culture. (a) ROS monitored by DHE (red) and nuclei by DAPI (blue) staining in PCa xenografts (scale bars, 50 μm). (b) MDA formation of PCa xenografts was examined after various treatments (c,d). PC-3 cells were treated with DDP, si-HIF-1α plasmid, or both, in the presence or absence of NAC (5 mM) or DHLA (0.25 mM) for 24 h. Total lysates (c) and culture media (d) were used to detect cellular H2O2 level. (e,f) Western analysis for HIF-1α as well as cleaved caspase-3 and PARP in PC-3 cells following various treatments. Data were presented as mean ± SD of three independent experiments. *p < 0.05 versus control group; #p < 0.05 versus si-HIF-1α or DDP group; $p < 0.05 versus DDP/si-HIF-1α group. The original blots are presented in Supplementary Figure 8. Image collected and cropped by CiteAb from the following open publication (https://www.nature.com/articles/s41598-017-07973-4), licensed under a CC-BY license. Not internally tested by Novus Biologicals.

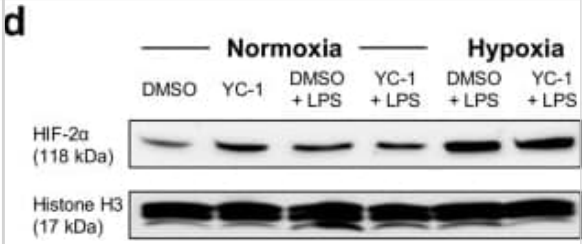

NDRG2 interacts with GLUT1. (A) SK-BR-3 cells were fixed and incubated with primary antibodies against N-myc downstream-regulated gene 2 (NDRG2) or glucose transporter 1 (GLUT1) and with fluorescein isothiocyanate or a cyanine 3 secondary antibody. Green fluorescence indicates NDRG2 expression, red fluorescence indicates GLUT1 expression and blue fluorescence indicates nuclear staining. The results of the merged images reveal that NDRG2 and GLUT1 were colocalised in the cytoplasm. (B) Immunoprecipitation (IP) assays were performed with whole-cell lysates of SK-BR-3 cells pretreated with protein A–conjugated sepharose beads. Whole-cell lysates were probed for input. The antibodies for immunoprecipitation and Western blot (WB) analyses were carried out as indicated. The locations of various proteins are indicated by arrowheads. IgG, Immunoglobulin G. Image collected and cropped by CiteAb from the following open publication (https://breast-cancer-research.biomedcentral.com/articles/10.1186/bcr3628), licensed under a CC-BY license. Not internally tested by Novus Biologicals.

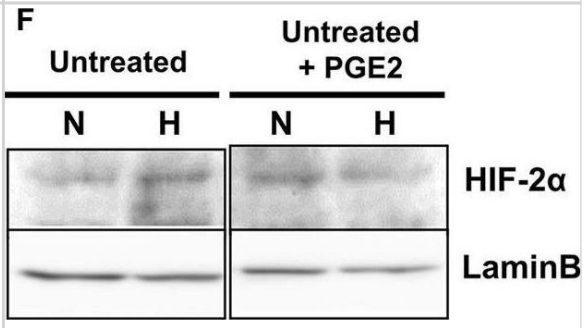

Expression of PACAP, VIP, VIPRs, HIF-1α, HIF-2α, and EGFR in glioblastoma multiforme (GBM). (A) Representative immunoblot of PACAP and VIP precursor peptides and PAC1R, VPAC1R, and VPAC2R expression on frozen glioblastoma sample. (B) Representative immunoblot and photomicrographs of signals detected by antibodies direct against HIF-1α, HIF-2α, and EGFR in a frozen glioblastoma sample. Image collected and cropped by CiteAb from the following open publication (https://journal.frontiersin.org/Article/10.3389/fphar.2016.00139/abstract), licensed under a CC-BY license. Not internally tested by Novus Biologicals.

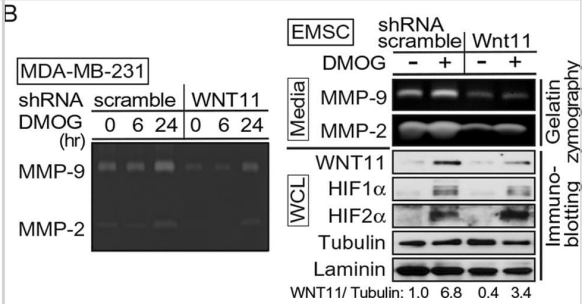

FCHSD1 and FCHSD2 immunolocalization in mouse cochlear hair cells.Shown are single confocal sections. FCHSD1 or FCHSD2 immunoreactivity visualized with Cy5 or FITC-conjugated secondary antibody was distinctly associated with stereocilia or cuticular plate, which were visualized with rhodamine-conjugated phalloidin. (A) FCHSD1 immunoreactivity in the cuticular plate of 3-week old mouse cochlear hair cells. (B) FCHSD1 immunoreactivity in the cuticular plate of 3-week old mouse outer hair cells. (C) FCHSD2 immunoreactivity in the hair bundles of 6-week old mouse cochlear hair cells. (D) FCHSD2 immunoreactivity in the hair bundles of 7-month old mouse inner hair cells. (E) FCHSD2 immunoreactivity in the hair bundles of 2-week old mouse outer hair cells. The Novus FCHSD1 antibody was used in (A) and (B). Scale bars: 10 µm in(A-C), 5 µm in (D) and (E). Image collected and cropped by CiteAb from the following open publication (https://pubmed.ncbi.nlm.nih.gov/23437151), licensed under a CC-BY license. Not internally tested by Novus Biologicals.	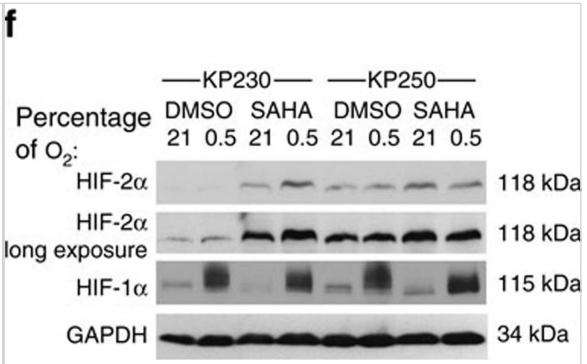
Spontaneously metastasizing tumor cells are more frequently doubly positive for dormancy and stem-like markers compared to intravenously injected tumor cells.a Representative images of triple immunofluorescence staining for GFP, NR2F1, and SOX9 expression in primary tumors, circulating tumor cells (CTCs), and disseminated tumor cells (Lung) from an E0771-GFP SM model (Left) and in disseminated tumor cells (Lung) from an EM model (Right). Green = GFP; Red = NR2F1; Orange = SOX9; Blue = DAPI. Scale bar for Primary Tumor = 50 µm. Scale bar for CTCs and Lung = 15 µm. b Percentage of double-positive tumor cells NR2F1-positive SOX9High from each group in Fig. 5a. Primary Tumor: n = 2383 in 97 fields of view (65 × 65 µm2) in 7 animals; CTCs: n = 379 cells in 8 animals; SM Lung: n = 104 cells in 9 animals; In vitro: n = 413 cells in 3 independent experiments. EM Lung: n = 75 cells in 7 animals. Bar = mean. Error bars = ±SEM. For EM Lung vs. SM Lung ($p = 0.0001$) and EM Lung vs. in vitro ($p = 0.69$), a two-tailed Kruskal-Wallis test with Dunn's multiple comparisons adjustment was used. For PT vs. CTC: ($p = 0.0041$), PT vs. Lung SM ($p = 0.0030$), and CTC vs. Lung SM ($p = 1.00$) a two-tailed ANOVA test with Sidak's multiple comparisons adjustment was used. **$p < 0.01$. ***$p < 0.001$. ns = not significant. Source data are provided as a Source Data file. Image collected and cropped by CiteAb from the following open publication (https://pubmed.ncbi.nlm.nih.gov/35110548), licensed under a CC-BY license. Not internally tested by Novus Biologicals.	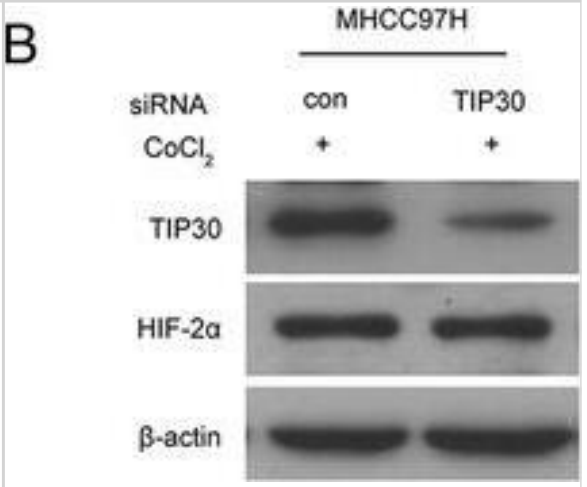
CIP2A downregulation reduces proliferation and induces apoptosis in melanoma cells. (A) The relative amount of viable cells measured by MTS assay 72 and 120 h post siRNA transfection. (B) Immunoblot analysis showing reduction in cancerous inhibitor of protein phosphatase 2A protein levels 48 h post siRNA transfection and effects on proliferation and apoptosis markers. The figure is representative of at last three independent biological experiments. Image collected and cropped by CiteAb from the following open publication (https://pubmed.ncbi.nlm.nih.gov/25663244), licensed under a CC-BY license. Not internally tested by Novus Biologicals.	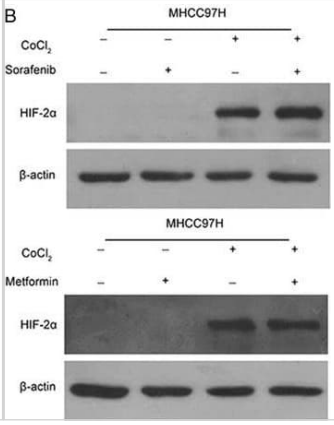

Elevated levels of additional proteins and GM3 ganglioside in the MEC of MPS IIIB brain.Staining performed with antibodies to the indicated substances was observed in the MEC region of 3 month-old MPS IIIB mice (for total ubiquitin and polyubiquitin) and 6 months for all others. Staining was not seen in the MEC region of age-matched control mice (Naglu +/−) nor in the LEC region of MPS IIIB mice (the latter not shown). Image collected and cropped by CiteAb from the following open publication (https://dx.plos.org/10.1371/journal.pone.0027461), licensed under a CC-BY license. Not internally tested by Novus Biologicals.	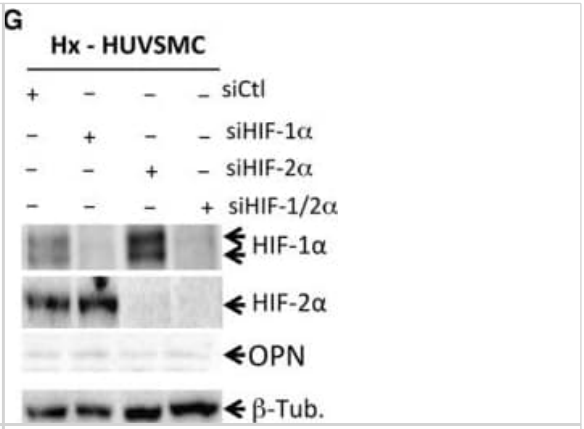
Transient hyperoxia does not sensitize normal human astrocytes to radiation.Results are shown for the colony forming assays for all previously assayed cell lines and a normal human astrocyte cell line (Astro). Cells were continuously maintained under normoxic conditions (NOx) or exposed to 25 min of hyperoxia (50% O2) and then returned to normoxic conditions for 25 min (HyperOx) before being treated with a 5 Gy dose of radiation. To allow for ease of comparisons among cell types, raw values are expressed as a percentage of the corresponding cells type's negative (non-irradiated) control and the means and SEMs are plotted. Each result represents three independent samples, plated in triplicate (*p<0.05, Student's t-test). Also shown are Western blots of nuclear HIF-1α at the time of irradiation for each cell line. Corresponding Western blots of lamin A/C are shown as a loading control. Image collected and cropped by CiteAb from the following open publication (https://pubmed.ncbi.nlm.nih.gov/25350400), licensed under a CC-BY license. Not internally tested by Novus Biologicals.	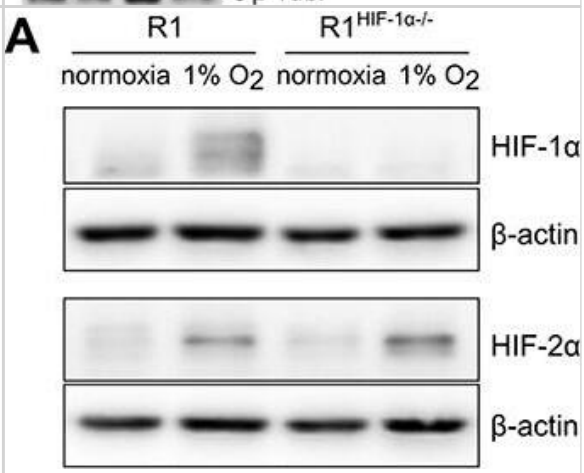
CIP2A is an inhibitor of PP2A-mediated DAPK dephosphorylationRSC96 cells were transfected with control, CIP2A siRNA (A), DKK-CIP2A (B), or DAPK siRNA (C) for 48 h and then exposed to GAS6 (100 ng/ml) for 30 min. PP2A activity and immunoblotting evaluations of DKK, CIP2A, pDAPK, and DAPK were performed. (D) RSC96 cells were incubated with GAS6 (100 ng/ml) for 30 min and co-immunoprecipitation between CIP2A, pDAPK and PP2A was evaluated. Immunoprecipitated PP2A activity was measured. Data are the mean ± SD, and n = 3 for each time point. * p < 0.05, ** p < 0.01, vs. control. Image collected and cropped by CiteAb from the following open publication (https://www.oncotarget.com/lookup/doi/10.18632/oncotarget.23978), licensed under a CC-BY license. Not internally tested by Novus Biologicals.	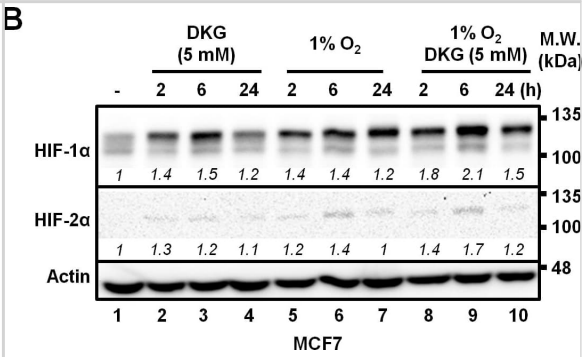

The BNIP3 C-terminus can be phosphorylated.(A) Western blot detection of immunoprecipitated BNIP3 using an α-PKA substrate antibody specific to the phosphorylated RRXS/T sequence, located at the BNIP3 C-terminus and adjacent to the transmembrane (TM) domain. Results shown for 4 cell types: (left to right) HEK 293 cells expressing exogenous BNIP3 (dimer, 60 kD), and A549, MDA-MD-231, and AU565 cells expressing endogenous BNIP3 (monomer, 30kD). Lane 1 of each Western blot contains the whole cell lysate (WCL). (B) LC-MS/MS analysis of BNIP3 phosphorylation in HEK 293 cells with normal or elevated cAMP (8-Bromo-cAMP), showing peptide coverage (gray) and phosphorylation sites (red). The TM domain is underlined. (C) Table of BNIP3 phosphopeptides identified by LC-MS/MS, showing the percent probability, ion charge, actual and observed masses, and mass error (Da and ppm) for each peptide. Peptides shown are from analysis of BNIP3 purified from HEK 293 cells with elevated cAMP levels. (D) Schematic of the BNIP3 protein sequence, showing each C-terminal mutation representing phosphomimetic or nonphosphorylated BNIP3. (E) Expression of BNIP3 phosphomutants from stable doxycycline-inducible HEK 293 Tet On cells, treated with doxycycline (Dox) for 48 hr. (F) Subcellular localization of BNIP3 phosphomutants, showing Western blot of cytosolic and mitochondrial fractions. (G) Alkaline extraction of mitochondria-associated proteins, showing alkaline extract of the mitochondrial pellet and the alkaline-resistant mitochondrial pellet from cells expressing each BNIP3 phosphomutant. All blots are representative of at least 3 independent experiments. Image collected and cropped by CiteAb from the following open publication (https://pubmed.ncbi.nlm.nih.gov/26102349), licensed under a CC-BY license. Not internally tested by Novus Biologicals.

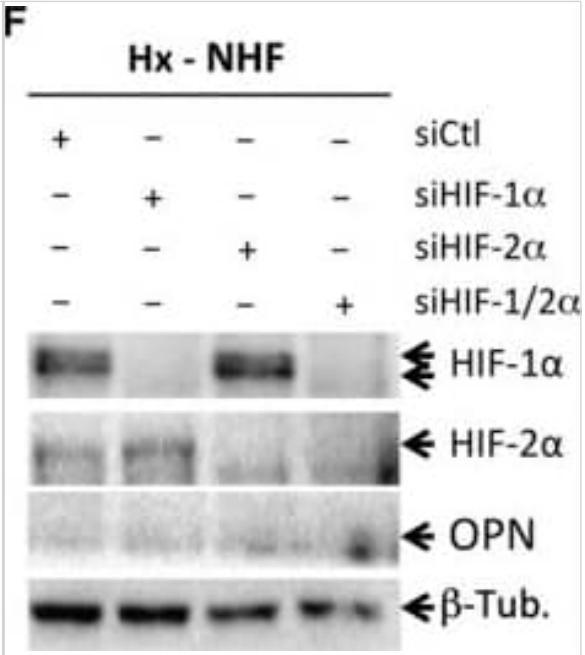

Expression of wild□type and ALS/FTD□mutant FUS reduces ER–mitochondria associations in NSC34 cellsAExpression of FUS does not alter expression of VAPB, PTPIP51 or mitofusin□2 (MFN2) in transfected NSC34 cells. Immunoblots of NSC34 cells transfected with EGFP as a control (CTRL), or wild□type or mutant EGFP□FUS. Transfected cells were purified via EGFP using a cell sorter and the samples probed on immunoblots as indicated. On the FUS immunoblot, samples were probed with FUS antibody to show endogenous and transfected proteins; tubulin is shown as a loading control.BRepresentative electron micrographs of ER–mitochondria associations in NSC34 cells transfected with control EGFP vector (CTRL), EGFP□FUS, EGFP□FUSR521C or EGFP□FUSR518K as indicated; arrowheads with loops show regions of association. Scale bar = 200 nm. Bar chart shows % of the mitochondrial surface closely apposed to ER in the different samples. Data were analysed by one□way analysis of variance (ANOVA) followed by Tukey's multiple comparison test. N = 27–30 cells and 247–424 mitochondria, error bars are s.e.m.; ***P < 0.001.C, DsiRNA loss of FUS does not affect ER–mitochondria associations or alter expression of VAPB, PTPIP51 or mitofusin□2 (MFN2) in NSC34 cells. (C) Immunoblots of cells either mock transfected or treated with control (CTRL) or FUS siRNAs; GAPDH is shown as a loading control. (D) Representative electron micrographs of ER–mitochondria associations in control (CTRL) and FUS siRNA□treated cells. Arrowheads with loops show regions of association. Scale bar = 200 nm. Data analysed by unpaired t□test. N = 27–28 cells and 193–202 mitochondria, error bars are s.e.m. Image collected and cropped by CiteAb from the following open publication (https://pubmed.ncbi.nlm.nih.gov/27418313), licensed under a CC-BY license. Not internally tested by Novus Biologicals.

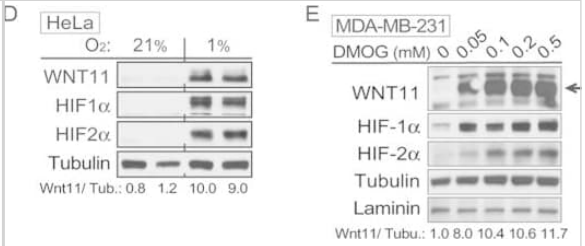

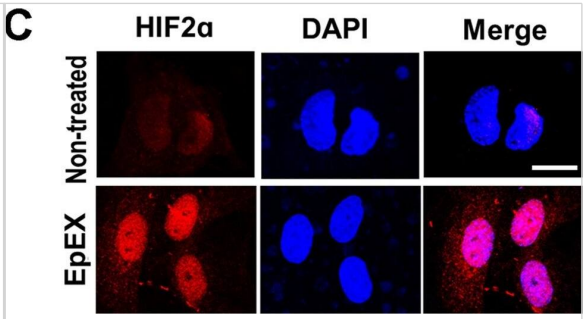

Motoneurons exhibit elevated Smn levels.(a–c) Single-cell immunofluorescent (scIF) experiments. 24 hpf pmnx1:eGFP embryos were dissociated and immunostained for Smn ((a) see also Methods). DIC image of cells following 3-hour (b) and 24-hour (c) incubation are shown with GFP in green. Note that the GFP signal in the cell body is oversaturated so that the weaker signal in the axon becomes visible. In (c) DNA is in blue and the motoneuron marker Znp1 (synaptotagmin) is in red; the axon growth cone is magnified in the corner of the images. Scale bars are 100 μm (a), 10 μm (low magnification in (b,c)) and 2 μm (high magnification in (c)). (d) scIF on pmnx1:eGFP embryos. Histone 2B (H2B), GFP and Smn signals are shown in Z-projected confocal sections. Cells marked by white rectangles are magnified on the right. Scale bars: 10 μm for low and 5 μm for high magnification. (e) To account for potential variability in the immunostaining, Smn levels were quantified relative to H2B. Diamonds denote GFP negative (GFP−) and GFP positive (GFP+) cells from one representative experiment. Blue bars indicate mean ± SD with significance values of *$p < 0.05$ and **$p < 0.01$. Exact values are (mean ± SD) 0.51 ± 0.14 (GFP−) and 0.87 ± 0.17 (GFP+), $p = 0.001$ with Wilcoxon Sum Rank Test. For more details, see Materials and Methods and Supplementary Table S1. (f) Average increase of Smn levels in motoneurons versus control cells. The exact value of enrichment is (mean ± SD): 1.67 ± 0.14. N = 3 experiments, n = number of analyzed cells. Image collected and cropped by CiteAb from the following open publication (https://www.nature.com/articles/srep27470), licensed under a CC-BY license. Not internally tested by Novus Biologicals.

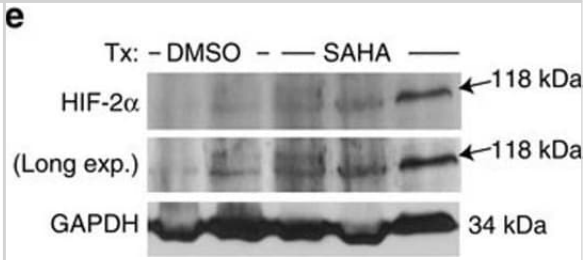

PML-RARa is a HIF-α transcriptional co-activator.A HIF-α transactivation assays (A–D) with HRE-luciferase construct. Results are presented as Luciferase/Renilla ratio (mean ± s.e.m. of experiments performed in triplicate).B HEK-293 cells transfected with stable mutants of HIF-1α or HIF-2α and increasing concentrations of PML-RARα.C HEK-293 cells transfected with a stable form of HIF-1α along with PML-RARα, PML or RARα.D Wild-type and Pml−/− MEFs transfected with HIF-1α and PML-RARα. Asterisks indicate fold change induction of HIF-1α-mediated transactivation upon PML-RARα expression.E HEK-293 cells transfected with the indicated fusion genes and treated with CoCl2.F Co-immunoprecipitation of exogenous stable forms of HIF-1α (left panel) and HIF-2α (right panel) and PML-RARα with a PML-directed antibody in HEK-293 cells. Of note, exogenously expressed PML-RARα migrates very closely to endogenous PML.Co-immunoprecipitation of endogenous HIF-1α and PML-RARα with a PML-directed antibody in NB4 cells treated with CoCl2.Data information: All experiments were repeated at least twice.Source data are available for this figure. Image collected and cropped by CiteAb from the following open publication (https://pubmed.ncbi.nlm.nih.gov/24711541), licensed under a CC-BY license. Not internally tested by Novus Biologicals.

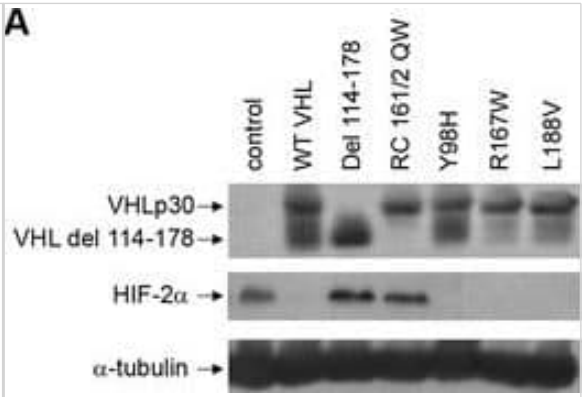

TAZ induces Tfam protein expression at the translational level.a The expression of mitochondrial biogenic factors, including Tfam, Ppargc1a (Pgc1α), Nrf1, and Nrf2, was analysed using quantitative reverse transcription (qRT)-PCR in the gastrocnemius muscle of wild-type (WT) and muscle-specific TAZ knockout (mKO) mice; n = 6 for each condition (Tfam; *p = 0.0498, Nrf1; *p = 0.0467). b Protein was analysed via immunoblotting to detect TAZ and the indicated mitochondrial biogenic factors in (a). Alpha-tubulin was used as the loading control. c RNA was isolated from the control (Con) and TAZ knockdown (KD) C2C12 myotubes, and the expression of the indicated mitochondrial biogenic factors was analysed using qRT-PCR. The experiments were performed in triplicate (Tfam; *p = 0.04). d Protein from the Con and TAZ KD C2C12 myotubes was assessed via immunoblotting to detect TAZ and mitochondrial biogenic factors. Beta-actin was used as the loading control. e RNA was isolated from WT, TAZ-knockout (KO), and TAZ-rescued (T) mouse embryonic fibroblasts (MEF), and the indicated mitochondrial biogenic factors were analysed via qRT-PCR. f Protein from WT, KO, and T MEF was assessed via immunoblotting to detect TAZ and the indicated mitochondrial biogenic factors. Beta-actin was used as the loading control. g Protein was isolated from the gastrocnemius muscle of WT and mKO mice and analysed via immunoblotting to detect TAZ, YAP, and proteins involved in the translation of both phosphorylated and total forms. Alpha-tubulin was used as the loading control. h Protein obtained from the Con and TAZ KD C2C12 myotubes was assessed via immunoblotting to observe TAZ and proteins involved in translation. Beta-actin was used as the loading control. i Protein was isolated from WT, KO, and T MEF and analysed via immunoblotting to detect TAZ and proteins involved in translation. Vinculin was used as the loading control. j The polysome profile of cells described in panel i was evaluated continuously by measuring absorbance at 254 nm. The 40S, 60S, 80S, and polysome fractions are denoted by the corresponding peaks. k The distribution of Tfam, Atp5d, and Gapdh mRNA from cells described in (j) across a density gradient was analysed using reverse transcription (RT)-PCR. bp = base pairs. For a, b, g 8 to 10-week-old mice were used. Data are presented as mean ± SEM for (a), mean ± SD for (c, e). Statistical significance was analysed via two-sided t-test for (a) and one-sided t-test for (c). One-way ANOVA with Tukey's multiple comparison test was used for (e). Representative data was shown and experiments were performed at least twice with similar results for (b, d, f–i, k). Source data are provided as a Source data file. Image collected and cropped by CiteAb from the following open publication (https://pubmed.ncbi.nlm.nih.gov/35115527), licensed under a CC-BY license. Not internally tested by Novus Biologicals.

Treatment with exogenous POT1 protein protects LT-HSCs in culture. a Effect of MTM-POT1a on colony formation of HSCs. LT-HSCs (8 week-old) were cultured with MTM-POT1a for 2 weeks. After culture, Lin− cells were isolated and re-cultured in MethoCult™ GF M3434 medium (200 cells per dish). Data are expressed as the mean ± SD (n = 3, *p < 0.01 by Tukey's test). Representative data from two independent experiments are shown. b, c LT-HSCs (8 week-old) were cultured with MTM-POT1a or control MTM protein. b Number of total cells and LT-HSCs on day 4, 7, and 10 of culture. Data are expressed as the mean ± SD (n = 6, *p < 0.01 by t-test). c Percentage of Annexin V+PI+ apoptotic cells in LT-HSCs on day 4, 7, and 10 of culture. Data are expressed as the mean ± SD (n = 6, *p < 0.01 by t-test). d LT-HSCs (8 week-old) were transduced with control shRNA or shPot1a-1. After 2 days of shRNA transduction, GFP+LT-HSCs were re-sorted and cultured with MTM-POT1a or control MTM protein. After 1 week of culture, Annexin V assay was performed. Percentage of Annexin V+PI+ apoptotic cells in GFP+LT-HSC fraction is shown. (n = 3, **p < 0.05 by Tukey's test). e Immunocytochemical staining of TRF (green), 53BP1 (red), and TOTO3 (blue) in 8 week-old LT-HSCs cultured for 3 weeks (left). Frequencies of TIFs after 3 weeks of culture (right). Data are expressed as the mean ± SD (n = 80–100, *p < 0.01 by t-test). f Representative FACS profiles of 8 week-old LT-HSCs after 3 weeks of culture with control MTM protein or MTM-POT1a (left). Numbers of LSK cells and LT-HSCs after 3 week culture (starting from 2400 cells) are shown in right panels. Data are expressed as the mean ± SD (n = 3, *p < 0.01 by t-test). Representative data from five independent experiments are shown Image collected and cropped by CiteAb from the following open publication (https://pubmed.ncbi.nlm.nih.gov/28986560), licensed under a CC-BY license. Not internally tested by Novus Biologicals.

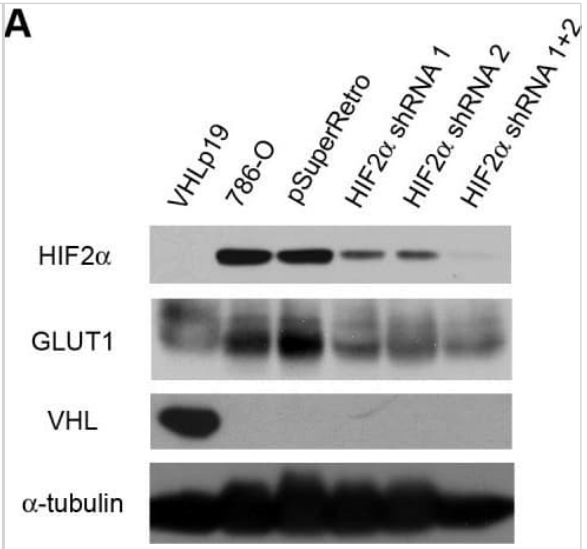

PGD2 is a paracrine mediator synthesized in myelinated large-diameter neurons that acts on TRPV1(+) neurons.(A) Dose-dependent induction of RII phosphorylation in sensory neurons after 1 min stimulation with PGD2 (EC50=377 nM, n=3,>2000 neurons/condition; one-way ANOVA with Bonferroni's multiple comparisons test). (B) PGD2 did not induce pRII in non-neuronal cells of the same cultures shown in A. (C) Time course of RII phosphorylation indicating long-lasting effects of PGD2 (10 μM) on sensory neurons. (D) Stimulation with PGD2 also results in phosphorylation of the ERK1/2 measured in the same cultures shown in D. (E) Representative experiment demonstrating that induction of RII phosphorylation is enhanced in TRPV1(+) neurons (total of 3664 neurons). Plots of respective controls are shown in S2 Fig. (F) Fold changes of pRII intensities in TRPV1(−) (grey bars) and TRPV1(+) (black bars) neurons after 1 min stimulation with 10 μM PGD2 (n=3,>2000 neurons/condition, one-way ANOVA with Bonferroni's multiple comparisons test). (G) Co-labeling of TRPV1 and PTGDS revealing that PTGDS is expressed in neurons lacking TRPV1 (total of 9951 neurons, also refer to S2 Fig. for control plots). (H) Co-labeling of NF200 and PTGDS showing that PTGDS(+) neurons express NF200 (total of 12966 neurons, also refer to S2 Fig. for control plots).(I) Size distribution of PTGDS(+) (green), NF200(+) (red), and all sensory neurons (black) indicating that PTGDS(+) neurons are larger than other neurons. (J) Suggested pathway of interneuronal communication between subgroups of sensory neurons. Large-diameter mechanosensitive neurons express PTGDS resulting in the production of PGD2, which activates DP1 receptors present on nociceptive neurons expressing TRPV1. Image collected and cropped by CiteAb from the following open publication (https://dx.plos.org/10.1371/journal.pone.0115731), licensed under a CC-BY license. Not internally tested by Novus Biologicals.

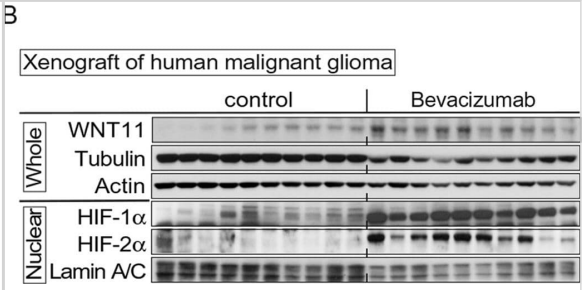

SPOC1 is recruited to I-SceI-induced DSBs where it colocalizes with 53BP1. (A) In situ immunofluorescence studies with U2OS19 ptight13 GFP-LacR cells with a stably integrated I-SceI cleavage site flanked by lac operator repeats reveals localization of the GFP-lac repressor protein (GFP-LacR) at the lac-operator DNA sequences in the nucleus before (−I-SceI) and 16 h after I-SceI-induced (+ I-SceI) DSB. In contrast, SPOC1 (white) and 53BP1 (red) are distributed throughout the nucleus in the absence of I-SceI, and partially colocalized in naturally occurring repair foci. After I-SceI cleavage to generate DSBs, SPOC1 and 53BP1 colocalize at distinct foci, including the cleaved DNA adjacent to DNA-bound GFP-LacR. Proteins were visualized by immunostaining and confocal microscopy. Scale bars = 10 μm. (B) Quantitative analysis of SPOC1 recruitment to the 53BP1 and GFP-LacR positive lacO array before and 16 h after I-SceI induction. (C) Monitoring of the kinetics of SPOC1 and 53BP1 recruitment to DSBs between 0 and 24 h post-I-SceI induction. (D) Quantifying ATM kinase inhibitor-mediated effects on recruitment of SPOC1 and 53BP1 to DSBs as evident 16 h after I-SceI-induced cleavage. (E) SPOC1 and 53BP1 colocalize at a large discrete endogenous repair focus as observed in some non-irradiated U2OS cells by immunostaining. Scale bar = 10μm. Image collected and cropped by CiteAb from the following open publication (https://academic.oup.com/nar/article-lookup/doi/10.1093/nar/gks868), licensed under a CC-BY license. Not internally tested by Novus Biologicals.

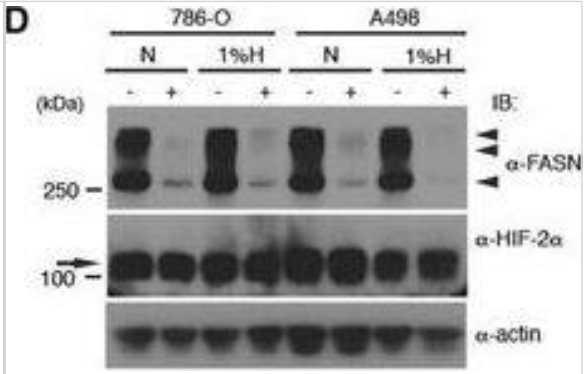

Hypoxia reduces inflammatory signaling pathways and NLRP3 expression and induces autophagy in IECs. a HT-29 cells were subjected to normoxia and hypoxia at the indicated times in the absence or presence of 10 μg/ml LPS. Autophagy was measured by variations in the ratio of LC3-II/LC3-I and the total amount of LC3 (LC3-I plus LC3-II) relative to β-actin. Results are representative of two independent experiments. b, c and d HT-29 cells were subjected to normoxia and hypoxia for the indicated periods in the absence or presence of 10 μg/ml LPS, followed by transcript analysis. Statistical analysis was performed using one-way ANOVA followed by Tukey's post-test. Results represent mean + s.e.m. of two independent experiments done in triplicate, *P < 0.05; **P < 0.01; ***P < 0.001; ns not significant. e HT-29 cells were subjected to normoxia or hypoxia in the presence and absence of 10 μg/ml LPS and 20 μM of MG132. Results are representative of two independent experiments. f and g Putative binding sites for HIF-1α and NF-κB were found in the p62 f and NLRP3 g promoters using Genomatix software tools. Numbers under the boxes indicate the distance from the transcription start site. HT-29 cells were subjected to normoxia (21% O2) or hypoxia (0.2% O2) for 6 h and 24 h. ChIP analysis was performed using antibodies against HIF-1α and NF-κB for immunoprecipitation. PCR was performed using the promoter-specific primers for the p62 f and NLRP3 g promoter binding sites of HIF-1α and NF-κB. Aliquots taken prior to immunoprecipitation were used as input control. PCR products were run on 2% agarose gel. The results are representative of three independent experiments. Image collected and cropped by CiteAb from the following open publication (https://pubmed.ncbi.nlm.nih.gov/28740109), licensed under a CC-BY license. Not internally tested by Novus Biologicals.

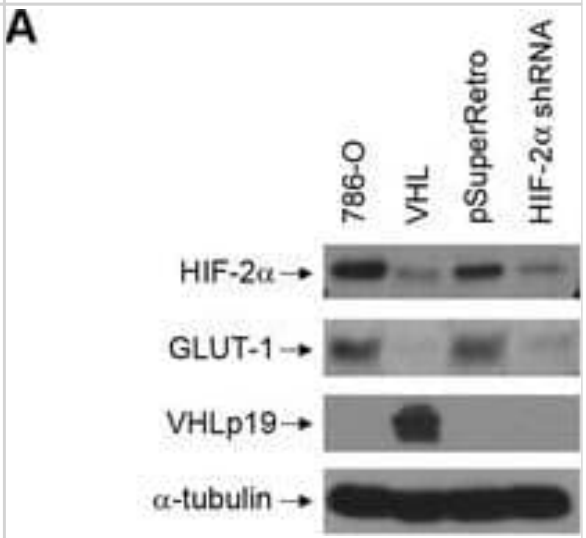

The FANCD2 NLS is required for the nuclear localization of a subset of FANCI.(A) FA-D2 patient cells or FA-D2 cells stably expressing FANCD2-WT were incubated in the absence (NT) or presence of MMC for 24 h, fixed, stained with rabbit polyclonal anti-FANCD2 or anti-FANCI antibody and counterstained with phalloidin and DAPI. AF-488, Alexa Fluor 488. (B) FA-D2 cells stably expressing LacZ, FANCD2-WT, FANCD2-ΔN57, FANCD2-ΔN100, and FANCD2-3N were incubated in the absence (NT) or presence of MMC for 24 h, fixed, and stained with rabbit polyclonal anti-FANCI antibody, and counterstained with phalloidin and DAPI. At least 300 cells were scored for cytoplasmic (Cyto.), nuclear (Nucl.), and both cytoplasmic and nuclear (Both) localization of FANCI. (C) COS-7 cells were transiently transfected with no DNA, FANCI-GFP, FANCI-GFP plus FANCD2-V5-WT, or FANCI-GFP plus FANCD2-V5-ΔN57. Whole-cell lysates were immunoprecipitated with anti-V5 or anti-GFP antibodies and immune complexes immunoblotted with anti-GFP and anti-V5 antibodies. Image collected and cropped by CiteAb from the following open publication (https://pubmed.ncbi.nlm.nih.gov/24278431), licensed under a CC-BY license. Not internally tested by Novus Biologicals.

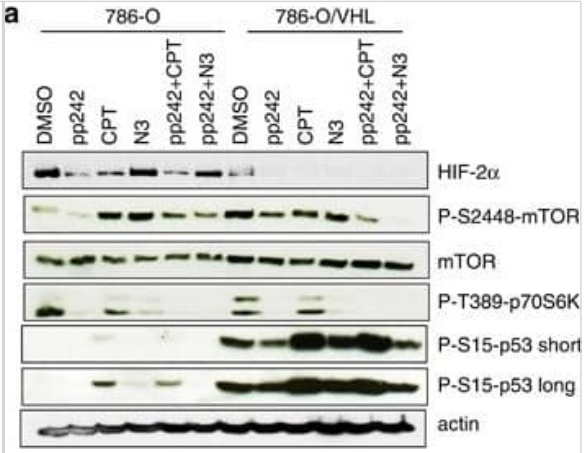

Analysis of microvascular density and HIF-1α activity. Microvascular density of pulmonary tumors was significantly higher in hyperplastic (B) and tumoral lesions (D) of NNK/NTHi treated mice compared to the NNK treated mice (A, and C) detected by CD105 immunostaining (10X, scale bar = 100 µm). HIF-1α immunostaining after NNK/NTHi combined treatment showed hot-spots of high stromal expression in tumors (F), and high expression in perivascular-peribronchiolar lymphocytes (H). In contrast, low, homogenous expression of HIF-1α was detected in the tumors (E) and perivascular-peribronchiolar lymphocytes (G) of NNK treated mice (40X, scale bar = 25 µm). Image collected and cropped by CiteAb from the following open publication (https://molecular-cancer.biomedcentral.com/articles/10.1186/1476-4598-11-4), licensed under a CC-BY license. Not internally tested by Novus Biologicals.

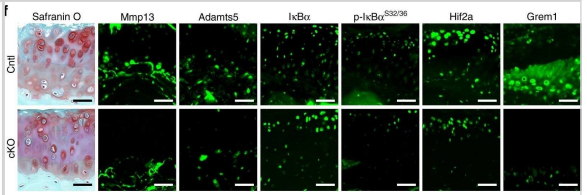

JMJD2B expression increases in hepatic steatotic cell and animal models. (A) HepG2 cells were incubated with a mixture of palmitic acid (PA) and oleic acid (OA) (1:2 ratio) at 800 µM concentrations for 24 h, and intracellular triglyceride (TG) levels were analyzed by a TG assay kit. JMJD2B mRNA and protein levels were examined by qPCR and western blotting, respectively. Data represent means ± SEM of three independent experiments performed in triplicate. *p < 0.05 vs. no treatment. The full-length western blots corresponding to truncated blots are presented in Supplementary Figure S1A. (B) HepG2 cells were treated with T0901317 (10 µM) for 24 h, and intracellular triglyceride (TG) levels were measured by a TG assay kit. JMJD2B mRNA and protein levels were examined by qPCR and western blotting, respectively. Data represent means ± SEM of three independent experiments performed in triplicate. *p < 0.05 vs. no treatment. The full-length western blots are presented in Supplementary Figure S1B. (C) Total RNAs were isolated from the livers of HFD-induced obese mice. The JMJD2B mRNA levels were assessed by qPCR. Data represent means ± SEM of 5 mice. *p < 0.05 vs. ND mice. ND: normal diet. HFD: high fat diet. Image collected and cropped by CiteAb from the following open publication (https://pubmed.ncbi.nlm.nih.gov/30214048), licensed under a CC-BY license. Not internally tested by Novus Biologicals.

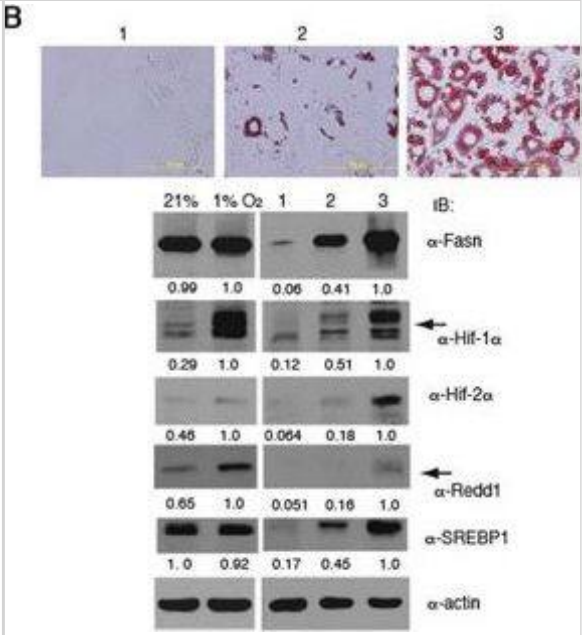

Protein expressions of intrarenal RAS components in two groups of mice. (A) Immunohistochemical analysis of intrarenal RAS expression position in the two groups of mice. AGT immunoreactivity in the proximal tubular cells, Ang II immunoreactivity in both glomerular and tubular cells, renin immunoreactivity in juxtaglomerular apparatus cells, ACE immunoreactivity in brush border membranes of proximal tubules as well as AT1 and AT2 immunoreactivity in the proximal tubules were increased in the HF group when compared to the control group. (B) Western blot analysis for protein expressions of intrarenal RAS components in the two groups of mice. (C) The histogram represents mean ± SD of the densitometric scans for the protein bands of angiotensinogen (AGT), angiotensin II (Ang II), renin, angiotensin converting enzyme (ACE), angiotensin II type 1 receptor (AT1), angiotensin II type 2 receptor (AT2) from five experiments, normalized by β-actin. * $P < 0.05$ vs. control. Image collected and cropped by CiteAb from the following open publication (https://pubmed.ncbi.nlm.nih.gov/23570453), licensed under a CC-BY license. Not internally tested by Novus Biologicals.

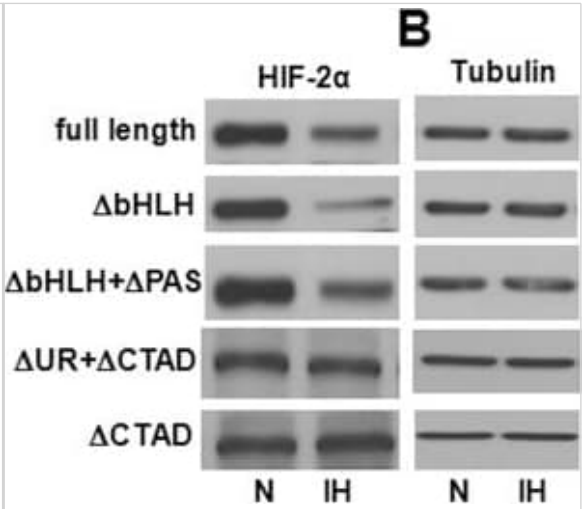

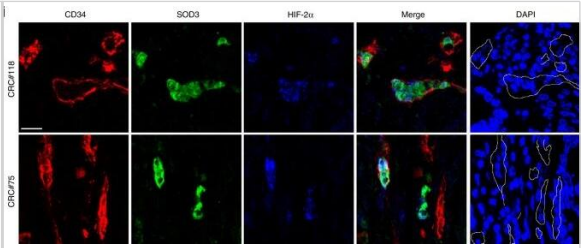

TAZ induces Tfam protein expression at the translational level.a The expression of mitochondrial biogenic factors, including Tfam, Ppargc1a (Pgc1α), Nrf1, and Nrf2, was analysed using quantitative reverse transcription (qRT)-PCR in the gastrocnemius muscle of wild-type (WT) and muscle-specific TAZ knockout (mKO) mice; n = 6 for each condition (Tfam; *p = 0.0498, Nrf1; *p = 0.0467). b Protein was analysed via immunoblotting to detect TAZ and the indicated mitochondrial biogenic factors in (a). Alpha-tubulin was used as the loading control. c RNA was isolated from the control (Con) and TAZ knockdown (KD) C2C12 myotubes, and the expression of the indicated mitochondrial biogenic factors was analysed using qRT-PCR. The experiments were performed in triplicate (Tfam; *p = 0.04). d Protein from the Con and TAZ KD C2C12 myotubes was assessed via immunoblotting to detect TAZ and mitochondrial biogenic factors. Beta-actin was used as the loading control. e RNA was isolated from WT, TAZ-knockout (KO), and TAZ-rescued (T) mouse embryonic fibroblasts (MEF), and the indicated mitochondrial biogenic factors were analysed via qRT-PCR. f Protein from WT, KO, and T MEF was assessed via immunoblotting to detect TAZ and the indicated mitochondrial biogenic factors. Beta-actin was used as the loading control. g Protein was isolated from the gastrocnemius muscle of WT and mKO mice and analysed via immunoblotting to detect TAZ, YAP, and proteins involved in the translation of both phosphorylated and total forms. Alpha-tubulin was used as the loading control. h Protein obtained from the Con and TAZ KD C2C12 myotubes was assessed via immunoblotting to observe TAZ and proteins involved in translation. Beta-actin was used as the loading control. i Protein was isolated from WT, KO, and T MEF and analysed via immunoblotting to detect TAZ and proteins involved in translation. Vinculin was used as the loading control. j The polysome profile of cells described in panel i was evaluated continuously by measuring absorbance at 254 nm. The 40S, 60S, 80S, and polysome fractions are denoted by the corresponding peaks. k The distribution of Tfam, Atp5d, and Gapdh mRNA from cells described in (j) across a density gradient was analysed using reverse transcription (RT)-PCR. bp = base pairs. For a, b, g 8 to 10-week-old mice were used. Data are presented as mean ± SEM for (a), mean ± SD for (c, e). Statistical significance was analysed via two-sided t-test for (a) and one-sided t-test for (c). One-way ANOVA with Tukey's multiple comparison test was used for (e). Representative data was shown and experiments were performed at least twice with similar results for (b, d, f–i, k). Source data are provided as a Source data file. Image collected and cropped by CiteAb from the following open publication (https://pubmed.ncbi.nlm.nih.gov/35115527), licensed under a CC-BY license. Not internally tested by Novus Biologicals.

Binding of TRF2 to viral DNA during HHV-6A/B infection.A) Schematic representation of the HHV-6A/B genome. The DR6 probe used for hybridization is shown in red. Uninfected and HHV-6A-infected HSB-2 cells (B-D) or uninfected and HHV-6B-infectd Molt-3 cells (E-F) were analyzed for TRF2 binding to viral DNA using ChIP. The input was hybridized with Alu probe to assess quantity of starting material. Anti-IgG (negative control), anti-PolII (positive control) or TRF2 antibodies were used for immunoprecipitation. B) QPCR detection of GAPDH DNA following ChIP. Results are expressed as fold increase over control IgG. C and E) Eluted DNA was hybridized with 32P-labeled Alu, telomeric (TTAGGG)3 or HHV-6A (DR6) probes. After hybridization the membranes were washed and exposed to X-ray films. D and F) Densitometric analysis of relative binding of TRF2 to telomeric and viral DNA. Results of one experiment representative of three are presented and are expressed as signal after normalization to input. Image collected and cropped by CiteAb from the following open publication (https://pubmed.ncbi.nlm.nih.gov/32320442), licensed under a CC-BY license. Not internally tested by Novus Biologicals.

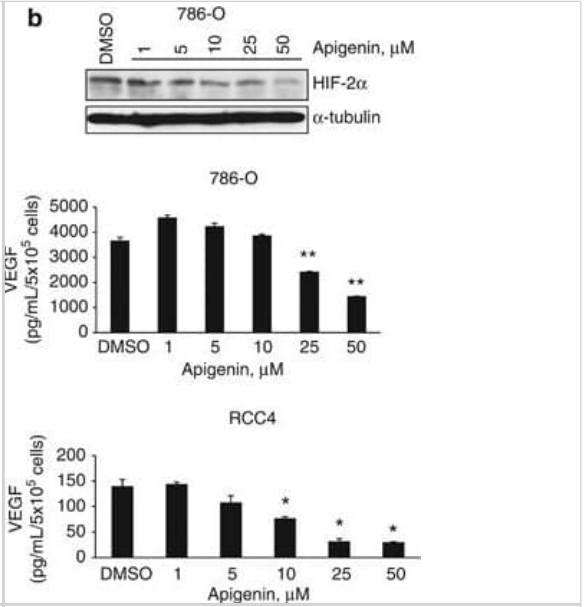

miR-375 control on CIP2A-MYC pathway also contributes to p21 elevation. (A) p21, p53, RB, CIP2A, and MYC protein levels in MCF7 cells transfected with miR-375 inhibitor, -mimic, or NS control were measured by Western blot analysis. Tubulin expression was used as internal control. 25%, 50%, 100% amounts of untreated cell lysates were included to calibrate the semiquantitative measurement. (B) Transfection with miR-375-mimic significantly upregulated p21 mRNA in MCF7. Relative endogenous p21 mRNA levels were measured in MCF7 cells transfected with miR-375 inhibitor, -mimic, or NS control for 48 h using qRT-PCR. (C) CIP2A and MYC protein levels were effectively silenced by si-CIP2A transfection with 1 and 10 nM concentrations for 48 h. Increased p21 protein levels were detected in si-CIP2A dose-dependent manner. 10 nM of si-GFP was used as a control. (D) Protein levels of CIP2A, p53, and p21 in MCF7 cells transfected with si-p53 and/or miR-375-mimic were measured by Western blot analysis. (E) mRNA levels of p21 in MCF7 cells transfected with si-p53 and/or miR-375-mimic were measured by qRT-PCR. (F) Flow cytometry analysis demonstrates G1 arrest of MCF7 cells 48 h after transfection with miR-375-mimic compared to miR-375 inhibitor or NS control. The concentrations of siRNA or miRNA used in panels D, E, and F were 10 nM and 25 nM, respectively. (G) Schematic depiction of miR-375-mediated repression of CIP2A, E6, E6AP, and E7 in HPV16-positive cells that simultaneously increases tumor suppressor p53, p21, and RB, and causes cell cycle arrest. Results are expressed as mean ± SD from three independent experiments. *p < 0.05, **p < 0.01, and ***p < 0.001. Image collected and cropped by CiteAb from the following open publication (https://pubmed.ncbi.nlm.nih.gov/24708873), licensed under a CC-BY license. Not internally tested by Novus Biologicals.

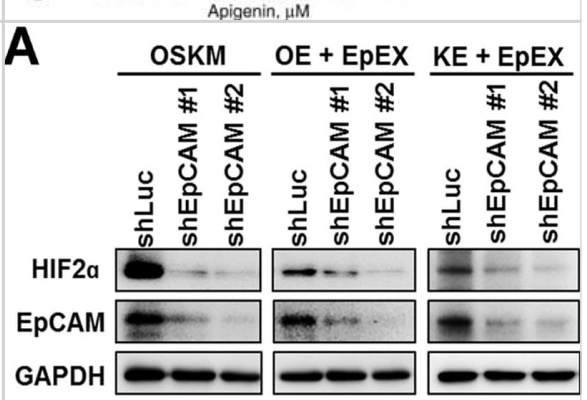

Effect of the four most common herbal formulas and single herbs on the phosphorylation of myosin light chain (MLC) protein.Briefly, A10 cells were treated with herbal formulas (A) or single herbs (B). Y27632 (Y10; 10 μM) and calyculin A (A50; 50 μg/ml) were used as negative and positive controls. Western blot analysis and staining with anti-phospho-MLC, anti-total-MLC, and anti-beta actin antibodies was then performed. Phospho-MLC, total-MLC, and beta actin were all obtained with their appropriate protein size bands. The relative Phospho-MLC intensity (%) was expressed as [(Phospho-MLC/total-MLC)drug treated/ (Phospho-MLC/total-MLC)cell only x 100%]. The Mean±SEM values for at least three independent experiments along with the representative western blot were performed. Image collected and cropped by CiteAb from the following open publication (https://dx.plos.org/10.1371/journal.pone.0145109), licensed under a CC-BY license. Not internally tested by Novus Biologicals.

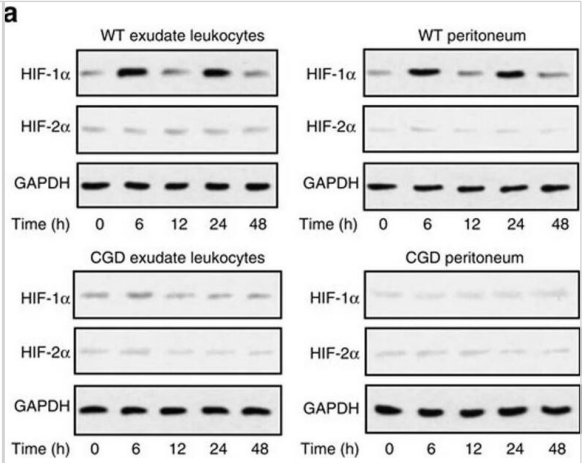

Silencing CIP2A caused decreased Cdk1 and Cdk2 proteins in 16E6□expressing cells. A, Western blot analysis of CIP2A, Cdk4, Cdk6, cyclin D1, Cdk1, Cdk2, cyclin B1, cyclin A2 and cyclin E1 protein levels in cells expressing HPV□16E6 transfected with CIP2A siRNA and then treated with PBS or 10 μg/mL bleomycin for 24 h. A representative of 3 independent experiments is shown. B, Quantification of all cell cycle□related proteins. Data from 3 experiments are summarized. C, Relative mRNA levels of all cell cycle□related genes determined by qRT□PCR. Data from 3 experiments are summarized. *, P < .05; **, P < .01 Image collected and cropped by CiteAb from the following open publication (https://pubmed.ncbi.nlm.nih.gov/29893470), licensed under a CC-BY license. Not internally tested by Novus Biologicals.

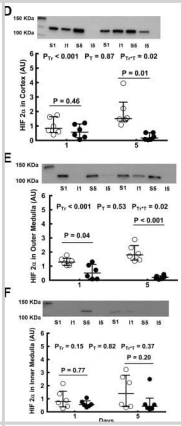

Effect of alcohol on TERT expression in liver tissues and KCs during ALD development.(a) TERT expression in liver tissues was performed by IHC analysis. Representative views from each group were presented (original magnification, ×40). (b) Total TERT mRNA and protein levels in liver tissue were analyzed by real-time PCR and western blot. The results are shown as relative expression against control expression without treatment. (c) Representative colocalization of TERT with macrophage CD68 immunoreactivity in liver tissue by using the double immunofluorescent (IF) analysis. (d) Total TERT mRNA and protein levels in KCs isolated from the liver were analyzed by real-time PCR and western blot. The results are shown as relative expression against control expression without treatment. (e) Quantification of telomerase activity (TA) in CD-fed mice and EtOH-fed mice. RNase treatment or heat inactivation of KCs isolated from the liver of EtOH-fed mice served as negative controls for the TA assay. All quantitative data are presented as mean ± SD percentage increase compared with CD-fed group (n = 4 in CD-fed group, n = 6 in EtOH-fed group) *P < 0.05, **P < 0.01 vs CD-fed group. Image collected and cropped by CiteAb from the following open publication (https://pubmed.ncbi.nlm.nih.gov/26725521), licensed under a CC-BY license. Not internally tested by Novus Biologicals.

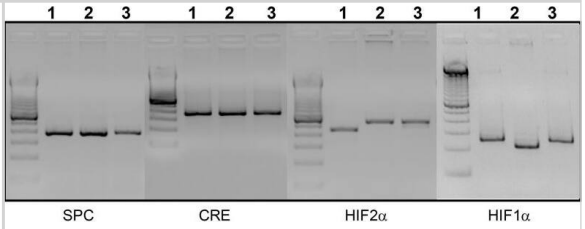

Publications

Ting KKY Lipid Loading of Macrophages Repurposes NADPH Metabolism to Suppress Glycolysis and Inflammation Thesis 2023-01-01

Bernstein I, Nixon B, Lyons J et al. The hypoxia-inducible factor EPAS1 is required for spermatogonial stem cell function in regenerative conditions iScience 2023-12-01 [PMID: 38077147] (IHC, Mouse)

Details:
Mouse testis

Yin H Chronic Hypoxia Impairs Skeletal Muscle Repair via HIF-2? Stabilization https://www.authorea.com/ 2023-10-02 (IHC, Mouse)

Contenti J, Guo Y, Larcher M et al. HIF-1 inactivation empowers HIF-2 to drive hypoxia adaptation in aggressive forms of medulloblastoma bioRxiv : the preprint server for biology 2023-10-20 [PMID: 37905067] (WB, Human)

Henning Y, Willbrand K, Larafa S et al. Cigarette smoke causes a bioenergetic crisis in RPE cells involving the downregulation of HIF-1? under normoxia Cell death discovery 2023-10-25 [PMID: 37880219] (WB, Human)

Zhang F, Zhang B, Wang Y et al. An extra-erythrocyte role of haemoglobin body in chondrocyte hypoxia adaption Nature 2023-10-01 [PMID: 37794190] (WB, Mouse)

Ting KKY, Yu P, Dow R et al. Oxidized Low-Density Lipoprotein Accumulation Suppresses Glycolysis and Attenuates the Macrophage Inflammatory Response by Diverting Transcription from the HIF-1? to the Nrf2 Pathway Journal of immunology (Baltimore, Md. : 1950) 2023-09-27 [PMID: 37756544]

Alexander KA, Yu R, Skuli N et al. Nuclear speckles regulate HIF-2? programs and correlate with patient survival in kidney cancer bioRxiv : the preprint server for biology 2023-09-16 [PMID: 37745397] (WB, ChIP, Mouse)

Qu M, Long Y, Wang Y et al. Hypoxia Increases ATX Expression by Histone Crotonylation in a HIF-2?-Dependent Manner International Journal of Molecular Sciences 2023-04-11 [PMID: 37108194] (B/N)

Sun D, Lu F, Sheldon A et al. Neuronal deficiency of hypoxia-inducible factor 2? increases hypoxic-ischemic brain injury in neonatal mice Journal of Neuroscience Research 2021-11-01 [PMID: 34487578]

Tiwari R, Bommi PV, Gao P et al. Chemical inhibition of oxygen-sensing prolyl hydroxylases impairs angiogenic competence of human vascular endothelium through metabolic reprogramming iScience 2022-10-21 [PMID: 36157579] (Func)

Wakefield ZR, Tanaka M, Pampo C et al. Normal tissue and tumor microenvironment adaptations to aerobic exercise enhance doxorubicin anti-tumor efficacy and ameliorate its cardiotoxicity in retired breeder mice Oncotarget 2021-08-31 [PMID: 34504647]

More publications at http://www.novusbio.com/NB100-122

Procedures

Western Blot protocol for HIF-2 alpha/EPAS1 Antibody (NB100-122)
General considerations for Western blot analysis of HIF-alpha proteins

1. HIF-2alpha is degraded under normoxic conditions and it is stabilized at O2 concentrations below 5% or with treatment using certain agents (CoCl2, DFO, etc.).

2. Positive and negative controls should always be run side by side in a Western blot to accurately identify the protein band upregulated in the hypoxic sample.

3. (HepG2 Hypoxic (CoCl2)/Normoxic Cell Lysate: NBP2-36451; HepG2 Hypoxic/Normoxic Cell Lysate: NBP2-36453).

4. To accurately compare treated and untreated samples and to ensure equal loading of samples the expression of a loading control should be evaluated.
(alpha Tubulin Antibody (DM1A): NB100-690)

5. The fully post-translationally modified form of HIF-2alpha is ~118 kDa, or larger.

6. HIF-2alpha may form a heterodimer with HIF-1beta. However, this is not typically seeing under denaturing conditions.

Western Blot Protocol

Materials

1x Laemmli Sample Buffer: 2% SDS, 2.5% 2-mercaptoethanol (bME), 25% glycerol, 0.01% bromophenol blue, 62.5 mM Tris HC, pH 6.8

1X Running Buffer: 25 mM Tris-base, 192 mM glycine, 0.1% SDS. Adjust to pH 8.3

1X Transfer buffer (wet): 25 mM Tris-base, 192 mM glycine, 20% methanol.

1X TBS

TBST (1X TBS with 0.1% Tween-20)

Blocking solution: TBST with 5% non-fat dry milk

Rabbit polyclonal anti-HIF-2 alpha primary antibody (NB100-122) in blocking solution (~1-2 ug/mL)

Methods

Whole-Cell Lysates

1. Load samples of treated and untreated cell lysates, 10-40 mg of total protein per lane on a 7.5% polyacrylamide gel (SDS-PAGE). Alternatively, gradient gels can be used for better resolution of lower molecular weight loading controls.

2. Resolve proteins by electrophoresis as required.

3. Transfer proteins to 0.45 mm PVDF membrane for 1 hour at 100V or equivalent.

4. Stain the blot using Ponceau S for 1-2 minutes to confirm efficient protein transfer onto the membrane.

5. Rinse the blot in distilled water to remove excess stain and mark the lanes and locations of molecular weight markers using a pencil.

6. Block the membrane using Blocking solution for 1 hour.

7. Dilute the rabbit anti-HIF-2 alpha primary antibody (NB100-122) in blocking solution (1-2 ug/ml) and incubate 1 hour at room temperature or overnight at 4oC.

8. Wash the membrane 3X 10 min in TBST.

9. Incubate in the appropriate diluted rabbit-IgG HRP-conjugated secondary antibody in blocking solution (as per manufacturer's instructions) for 1 hour at room temperature.

10. Wash the membrane 3X10 min in TBST.

11. Apply the detection reagent of choice in accordance with the manufacturer's instructions (e.g., ECL, ECL Plus). Image blot.

Immunocytochemistry/Immunofluorescence protocol for HIF-2 alpha/EPAS1 Antibody (NB100-122)
HIF-2 alpha/EPAS1 Antibody:
Immunocytochemistry Protocol

Culture cells to appropriate density in 35 mm culture dishes or 6-well plates.

1. Remove culture medium and wash the cells briefly in PBS. Add 10% formalin to the dish and fix at room temperature for 10 minutes.
2. Remove the formalin and wash the cells in PBS.
3. Permeablize the cells with 0.1% Triton X100 or other suitable detergent for 10 min.
4. Remove the permeablization buffer and wash three times for 10 minutes each in PBS. Be sure to not let the specimen dry out.
5. To block nonspecific antibody binding, incubate in 10% normal goat serum from 1 hour to overnight at room temperature.
6. Add primary antibody at appropriate dilution and incubate overnight at 4C.
7. Remove primary antibody and replace with PBS. Wash three times for 10 minutes each.
8. Add secondary antibody at appropriate dilution. Incubate for 1 hour at room temperature.
9. Remove secondary antibody and replace with PBS. Wash three times for 10 minutes each.
10. Counter stain DNA with DAPi if required.

Novus Biologicals USA
10730 E. Briarwood Avenue
Centennial, CO 80112
USA
Phone: 303.730.1950
Toll Free: 1.888.506.6887
Fax: 303.730.1966
nb-customerservice@bio-techne.com

Bio-Techne Canada
21 Canmotor Ave
Toronto, ON M8Z 4E6
Canada
Phone: 905.827.6400
Toll Free: 855.668.8722
Fax: 905.827.6402
canada.inquires@bio-techne.com

Bio-Techne Ltd
19 Barton Lane
Abingdon Science Park
Abingdon, OX14 3NB, United Kingdom
Phone: (44) (0) 1235 529449
Free Phone: 0800 37 34 15
Fax: (44) (0) 1235 533420
info.EMEA@bio-techne.com

General Contact Information
www.novusbio.com
Technical Support: nb-technical@bio-techne.com
Orders: nb-customerservice@bio-techne.com
General: novus@novusbio.com

Products Related to NB100-122

NB800-PC26	COS-7 Nuclear Hypoxic Induced Cell Lysate
HAF008	Goat anti-Rabbit IgG Secondary Antibody [HRP]
NB7160	Goat anti-Rabbit IgG (H+L) Secondary Antibody [HRP]
NBP2-24891	Rabbit IgG Isotype Control

Limitations
This product is for research use only and is not approved for use in humans or in clinical diagnosis. Primary Antibodies are guaranteed for 1 year from date of receipt.

For more information on our 100% guarantee, please visit www.novusbio.com/guarantee

Earn gift cards/discounts by submitting a review: www.novusbio.com/reviews/submit/NB100-122

Earn gift cards/discounts by submitting a publication using this product: www.novusbio.com/publications